

Evaluation of Phenol-Substituted Diphyllin Derivatives as Selective Antagonists for Ebola Virus Entry

Caroline B. Plescia,[#] Aaron R. Lindstrom,[#] Maritza V. Quintero, Patrick Keiser, Manu Anantpadma, Robert Davey, Robert V. Stahelin, and V. Jo Davison*



Cite This: *ACS Infect. Dis.* 2022, 8, 942–957



Read Online

ACCESS |



Metrics & More



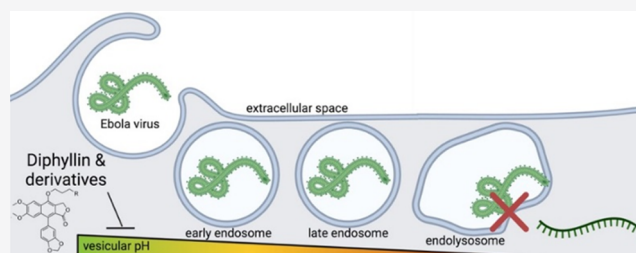
Article Recommendations



Supporting Information

ABSTRACT: Ebola virus (EBOV) is an aggressive filoviral pathogen that can induce severe hemorrhagic fever in humans with up to 90% fatality rate. To date, there are no clinically effective small-molecule drugs for postexposure therapies to treat filoviral infections. EBOV cellular entry and infection involve uptake via macropinocytosis, navigation through the endocytic pathway, and pH-dependent escape into the cytoplasm. We report the inhibition of EBOV cell entry via selective inhibition of vacuolar (V)-ATPase by a new series of phenol-substituted derivatives of the natural product scaffold diphyllin. In cells challenged with Ebola virus, the diphyllin derivatives inhibit viral entry dependent upon structural variations to low nanomolar potencies. Mechanistically, the diphyllin derivatives had no effect on uptake and colocalization of viral particles with endocytic marker LAMP1 but directly modulated endosomal pH. The most potent effects were reversible exhibiting higher selectivity than bafilomycin or the parent diphyllin. Unlike general lysosomotropic agents, the diphyllin derivatives showed no major disruptions of endocytic populations or morphology when examined with Rab5 and LAMP1 markers. The dilated vacuole phenotype induced by apilimod treatment or in constitutively active Rab5 mutant Q79L-expressing cells was both blocked and reversed by the diphyllin derivatives. The results are consistent with the action of the diphyllin scaffold as a selective pH-dependent viral entry block in late endosomes. Overall, the compounds show improved selectivity and minimal cytotoxicity relative to classical endosomal acidification blocking agents.

KEYWORDS: viral entry inhibitor, V-ATPase inhibitor, endosome trafficking, diphyllin, macropinocytosis



Filoviruses are a diverse family of lipid enveloped viruses that represent an ongoing concern for human health. Among the most prevalent is Ebola virus (EBOV), which caught global attention during a 2014–2016 outbreak with over 28,000 cases recorded in 10 countries and a fatality rate of approximately 40%.¹ Subsequent outbreaks in the Democratic Republic of the Congo and Guinea have resulted in more than 3000 cases and a case fatality of 67%. A preventative vaccine (Ervebo) and two monoclonal antibody-based therapeutics (Inmazeb and Ebanga) were recently FDA approved. Despite early promise, remdesivir proved to provide little efficacy in the clinic, and there remains no clinically effective small-molecule therapy.²

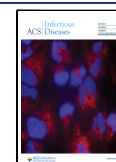
Many viral pathogens share common steps in viral entry, suggesting the potential for broad-spectrum therapies. Filoviral pathogens are negative-stranded RNA viruses that encode only a few enzymes considered traditional targets for inhibition. Viral entry into cells, where the virus first binds to cell surface receptors followed by endosomal trafficking before entering the cell cytoplasm, offers many important potential host targets. EBOV cell entry involves engagement of the virus particle with receptors that include TIM-1, which triggers uptake via macropinocytosis.^{3–7} EBOV viral particles use endosomes for delivery to lysosomes during which a reduction in pH activates

cathepsins to cleave the viral glycoprotein (GP).^{8,9} The processed form of GP can interact with the lysosomal host cell receptor, Niemann Pick C-type 1 (NPC1).^{10–13} This binding event, together with other environmental factors, is necessary for the eventual fusion of viral and vesicular membranes, releasing the viral contents into the cytoplasm where genome transcription and replication can initiate and produce new virus progeny.

Of interest for clinical translation are broad-spectrum viral entry inhibitors with known pharmacological mechanisms of action toward host targets. Agents targeting the required host factor NPC1 based on analogues of tetrandrine are under investigation, as are specific agents for the lysosomal NPC1 receptor.^{14,15} In the cases for known inhibitors of lipid kinases such as apilimod (PIKFyve)¹⁶ and R-59-022 (diacylglycerol kinase),¹⁷ understanding the contributions of on-target

Received: September 6, 2021

Published: March 31, 2022



mechanisms for blockage of viral entry could offer approaches to new antiviral agents.^{18,19} Many efforts have pursued drug repurposing as an approach to EBOV inhibitors, but developing these agents as antiviral therapies can present challenges for optimization.^{20–22} Previous research and screening efforts have identified alternative classes of inhibitors for EBOV entry.^{23–30}

To date, the improvement of EBOV inhibitor activities by structural modifications has been demonstrated only in select cases.^{31–33} However, the mechanisms of viral entry blockade by these agents remain unknown. Many EBOV entry inhibitors like chloroquine share chemical features associated with non-selective cationic amphiphilic drugs (CADs).³⁴ The antiviral drug effects of these agents are often considered off-target trapping in acidic vesicles and lysosomes.³⁵ The mechanisms by which these effects translate to inhibition of viral entry are unclear and remain challenging to optimize.

V-ATPases mediate acidification of endocytic vesicles by coupling ATP hydrolysis to proton pumping. Natural product inhibitors of V-ATPase like bafilomycin have shown utility as research tools for decades (Figure 1). The results with natural-

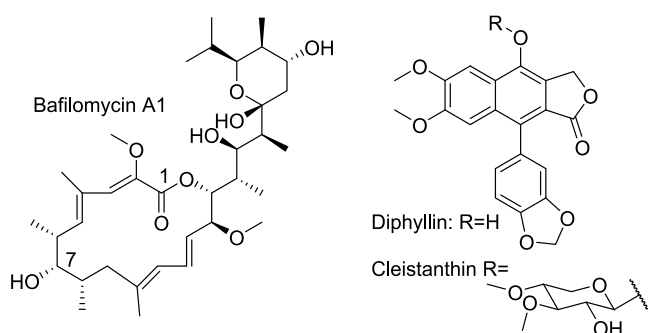


Figure 1. Natural-product-inspired V-ATPase inhibitors and/or other viral entry inhibitors.

product-inspired synthetic macrolide, SaliPhe, demonstrated the potential utility of a potent V-ATPase inhibitor to block viral entry.^{36–38} Despite being evaluated in disease models, these agents have been overlooked for clinical development primarily due to narrow selectivity. Diphyllin, a plant-derived aryl-naphthalene lactone chemotype member, is also a V-ATPase inhibitor. This compound and its derivatives have shown broad-spectrum and selective antiviral activity *in vitro* against dengue,^{39,40} HIV,⁴¹ EBOV and Marburg,⁴² SARS-CoV-2,⁴³ influenza,^{39,44,45} West Nile, Japanese encephalitis, and tick-borne encephalitis.⁴⁰ A nanoparticle formulation of diphyllin has shown *in vivo* antiviral activity against influenza⁴⁵ and coronavirus.⁴⁶ In a lethal Zika infection mouse model, the diphyllin-6-deoxyglucoside derivative showed significant *in vivo* antiviral activity.⁴⁰

In our prior work, we evaluated diphyllin structural analogues to define the significance of the lactone ring. These modifications of the diphyllin core substructure diminished inhibitory potency of the endosome acidification, V-ATPase turnover, and EBOV cell entry efficiency. However, diphyllin-ether derivatives showed improved selectivity suggesting that further chemical development could lead to better tolerated and broadly acting antiviral treatments.⁴² However, there remain large gaps in our understanding of what features could be exploited to enhance potency and selectivity while minimizing cytotoxicity. In addition, the underlying cellular mechanism of viral entry inhibition remains to be fully established. Here, we

evaluate a set of novel diphyllin-ether derivatives to further refine the structural features that impact endocytic pH, effects on EBOV trafficking, and improve potency for inhibition of EBOV into the low nanomolar range while maintaining a wide window of selectivity.

RESULTS AND DISCUSSION

Rationale for Target Compounds. A minimal survey of diphyllin scaffold modifications focusing on the lactone ring system was the subject of a previous publication.⁴² The results indicated a loss of activity for ring open variants of the aryl-naphthalene lactone. Extensions of the lactone ring system as hydrazones restored some biological activity, but this substitution proved not to be a robust path for further structural modifications to usefully active compounds. In contrast, the phenol substitution with simple alkyl ethers including methyl, ethyl, and butyronitrile provided compounds with improved potency for blocking viral entry and enhanced V-ATPase inhibitory activity. Interestingly, side chains bearing the cyclic base groups morpholino or hydroxyethylpiperazine also provided compounds with improved viral entry inhibition and selectivity with no observed toxicity in primary human macrophages (PHMs). Overall potency for both activities ranged from low micromolar to the hundreds of nanomolar.

A series of phenol-substituted ethers covering a relatively broad range of log *P* were pursued to follow up on the prior observations. In particular, the effects of the morpholino and piperazinyl groups in the side chain suggested a role for basic nitrogen groups in enhancing the potency of viral entry inhibition. The synthesis of ethers was established by a prior procedure using simple alkyl halides for a few extensions presented in Figure 2A to reveal compounds 1.2–1.6 in Table 1. This minimal set of compounds flanked the cLog *P* of diphyllin (3.34) with three compounds higher (4.06–4.55) and two lower in value (2.60 and 3.14). Alkylation of the phenolic position with bromoacetate followed by amidation (Figure 2B) was used to prepare derivatives with a hydrophilic linker in the side chain.

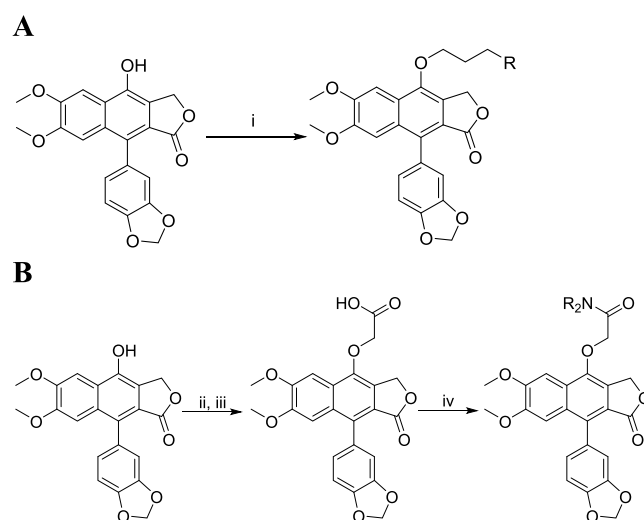
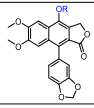
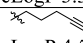
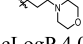
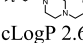
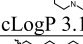
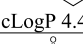
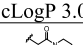
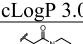
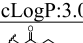
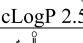
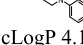
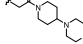
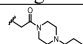
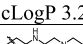
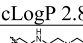
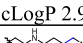
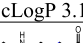
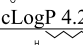
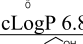
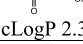


Figure 2. Synthetic scheme for alkyl and amide inhibitors. (A) (i) $\text{ClCH}_2\text{CH}_2\text{CH}_2\text{R}$, K_2CO_3 , dimethyl sulfoxide (DMSO), 3–16 h, 100 °C. (B) (ii) $\text{BrCH}_2\text{COOEt}$, K_2CO_3 , DMSO, 100 °C, 2 h; (iii) 0.2 M NaOH H_2O :IPA (1:4), rt, 16 h; and (iv) R_2NH , triethylamine (TEA), HCTU, *N,N*-dimethylformamide (DMF), 3 h, MW (irradiation), 100 °C.

Table 1. Evaluation of Diphyllin Analogues^{a,b,c}

ID		V-ATPase Inhibition IC ₅₀ (nM)	HEK293 AO IC ₅₀ (nM)	CC ₅₀ /IC ₅₀ HEK-293	^c EBOV-HeLa EC ₅₀ (nM)	CC ₅₀ /IC ₅₀ HeLa	^c EBOV-PHM EC ₅₀ (nM)	CC ₅₀ /EC ₅₀ PHM
Baf ^b	-	24.8±2.66	40.5±3.31	7.90	15±9	ND	ND	ND
1.1	H cLogP 3.34	189±1.66	476±60.1	37.4	815±195	33.4	1094±735	>250 ^b
1.2	 cLogP 4.55	16.9±3.72	102±19.0	39.6	246±18	50	990±422	>250 ^b
1.3	 cLogP 4.06	27.4±3.88	74.3±23.9	151	95±4	109	15±7	>1000 ^b
1.4	 cLogP 2.60	61.0±2.84	104±21.2	299	52±2	188	44±14	>500 ^b
1.5	 cLogP 3.14	5.86±0.94	0.356±0.03	208	20±1	1194	10±4	>1000 ^b
1.6	 cLogP 4.46	35.4±2.91	338±81.8	190	246±15	>103 ^b	201±44	>200 ^b
1.7	 cLogP 3.05	460±33.6	3,710±845	>27.0	1,673±490	4.8	ND	
2.1	 cLogP 3.06	17.9±3.30	245±32.7	>408	217±57.6	>45 ^b	ND	
2.2	 cLogP:3.01	4.02±0.698	166±18.9	>602	563±75.6	>44 ^b	ND	
2.3	 cLogP 2.58	8.91±3.29	411±63.1	>243	1,620±190	>15 ^b	ND	
2.4	 cLogP 4.11	150±31.3	440±59.3	>227	564±59.1	>56 ^b	ND	
2.5	 cLogP 3.31	33.3±5.02	271±60.3	>369	1,690±330	>12 ^b	ND	
2.6	 cLogP 3.26	14.8±3.19	140±23.4	>714	1,755±263	>14 ^b	ND	
2.7	 cLogP 2.87	7.19±1.06	448±73.3	>223	2,901±256	>8.6 ^b	ND	
2.8	 cLogP 2.92	14.2±2.5	2,410±705	31.8	2,624±344	>9.5 ^b	ND	
2.9	 cLogP 3.14	11.5±1.23	4,300±1,110	>23.3	3,888±700	>6.4 ^b	ND	
2.10	 cLogP 4.24	43.6±7.49	591±123	121	456±134	8.1	ND	
2.11	 cLogP 6.82	14.7±1.64	487±60.5	146	1,180±186	23.7	ND	
2.12	 cLogP 2.32	15.0±3.69	1,190±400	>84.0	532±37.1	11.6	ND	
2.13	 cLogP 4.2	68.2±12.0	391±33.0	57.5	339±61.9	20.3	ND	

^aData from ref 46. ^bNo effect on cell viability observed at 25 μM. ^cEBOV = replication competent Ebola virus; PHM = primary human macrophage; and CC₅₀ is for cytotoxicity after 3 day drug treatment. Baf = bafilomycin A1, entry 1.1 = diphyllin, and AO = acridine orange; all data have been tested in biological triplicates with different batches of compounds.

The two-step process provided additional structural modifications (2.1–2.13) that included alterations in ionizable basic groups in side chains with lower clog *P* values covering the range of 2.32–4.24.

Diphyllin and Derivatives Are Potent V-ATPase Inhibitors. The primary assays for all compounds followed a parallel experimental path to qualify the relative activities for: (a) V-ATPase activity in isolated endosomal vesicles, (b) in intact

HEK293 cells, and (c) inhibition of Ebola virus infection in HeLa cells (Table 1, Figures S1 and S2) and in HEK293 cells (Table S1). This series of phenol ethers comprising nitrogen-containing groups of varied p*K*_a and lipophilicity improved V-ATPase inhibition potency by the isolated vesicle assay. Several analogues gave activities equivalent to or better than bafilomycin. In cell-based endosome acidification assays, inhibitor potencies varied over 1000-fold and were reflected in

EBOV infection assays. The most potent and selective compounds bear a three-carbon aliphatic linker (1.3–1.6). Surprisingly, the less lipophilic acetamide linker diminished potency even when nitrogen heterocycles were similar. For example, the relative differences in cellular activities for 1.3–1.5 versus 2.1–2.3 indicate significant roles for spacer chain composition. Adding lipophilic and basic groups in the acetamide linker (2.4–2.9) further reduced potency to less than the parent diphyllin (1.1).

Diphyllin and Derivatives Inhibit Early Steps of Virus Infection. A time of addition assay was performed to gain further insight into the step at which the compounds may affect virus replication (Figure 3A). Compounds 1.1 and 1.5 start to

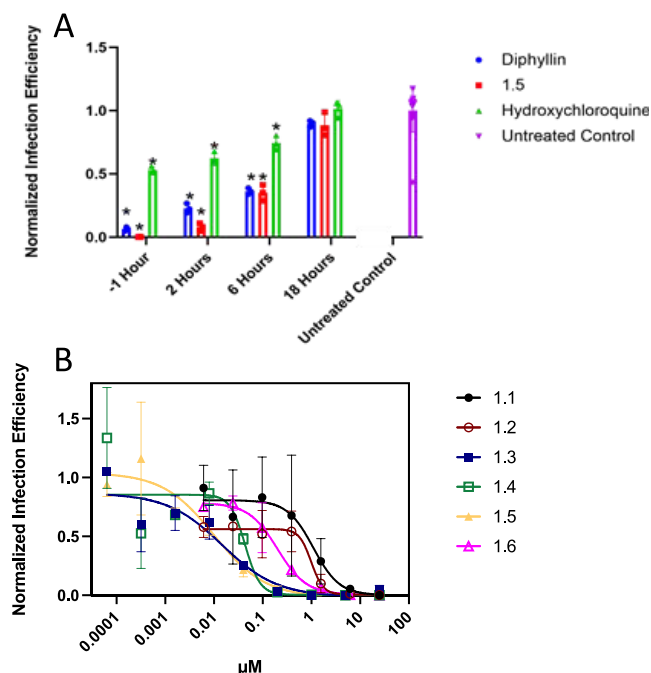


Figure 3. Time addition measurements of compound action and activity in primary human macrophages. (A) Time of addition of compounds indicates mechanism of action at early steps in virus replication. HeLa cells were pretreated for 1 h and then infected with wild-type EBOV or treated 2, 6, or 18 post infections. Cells were dosed with 1.5 (0.16 μM), 1.1 (2 μM), or 2 μM hydroxychloroquine. Infection efficiency was normalized to untreated controls, and one-way analysis of variance (ANOVA) was used to determine significance by $P < 0.05$ (*) between time points and the untreated controls. (B) EBOV infection in primary human macrophages. Primary human macrophages were infected with live GFP-EBOV after pretreatment with compounds for 1 h. Compounds were not removed before infection. Infected cells were fixed, stained, and imaged with epifluorescent microscopy, and infection efficiency was quantified by counting infected cells and normalizing to the total cell count in CellProfiler software. Prism 8 software was used to generate a graph, fit curves, and calculate IC_{50} values.

show diminished activity at 6 h and were ineffective at 18 h after virus addition to cells. This timeframe is consistent with a block at early steps of infection involving cell attachment through to endosomal escape of virus particles into the cell cytoplasm. Despite being active when the virus requires V-ATPase activity to acidify endosomes to promote infection, the trend in potencies did not correlate with the IC_{50} values in the isolated vesicle V-ATPase assay (Pearson correlation $r = -0.09$, Figure S3). The potential for compound degradation in the cell culture

media was evaluated for a representative number of the acetamide side chain compounds (Figures S4 and S5) to assess if poor stability could explain the diminished cellular activities. For the most rapidly degraded compound 2.3, the lifetime of the parent molecule would be $>70\%$ during the endosome acidification assay time course. These changes in compound concentrations would not explain the minimal activities. In addition, cell-based assays for endosome acidification and the EBOV entry all showed meaningful correlations of the potencies (Figure S3). While a significant correlation exists between EBOV entry assays in two cell lines, the margin of error of the assays conducted using HEK293 cells was larger than that in HeLa cells. HEK293 cell loss from poor adherence contributes to reduced overall quality and significance of the pharmacological test (Table S1). In general, the performance of compounds in HEK293 cells was less potent (5–10-fold) than that of seen in HeLa cells. The reason for this difference is unclear but may relate to the types of V-ATPase being expressed or differences in endocytic turnover. Despite this difference, the relative potencies of the analogues were similar to those observed in the HeLa cell entry data and gave a positive correlation ($r = 0.63$, $P = 0.005$).

Diphyllin and Derivatives Are Active against EBOV Infection in Primary Human Macrophages. Filoviral infection of macrophages is considered one of the primary routes of establishing and continuing disease.^{47–49} The promising activity of compounds 1.2–1.6 in HeLa cells prioritized evaluation in PHMs. Compounds were preincubated for 1 h with PHMs before challenge with recombinant Ebola virus encoding GFP as a marker of infection (GFP-EBOV). At 24 h post infection, the number of infected (GFP⁺) cells was counted with epifluorescence imaging. A dose dependency was calculated for each compound and normalized to the DMSO vehicle control (Figure 3B). Compounds 1.3–1.6 bear a basic nitrogen heterocycle in the side chain and exhibited improved potencies and selectivities with respect to 1.1–1.2. Compound 1.5 ($\text{pK}_{\text{a}1}$ 8.92, $\text{pK}_{\text{a}2}$ 3.79) showed enhanced potency in blocking acidification of isolated vesicles and live-cell endosomes, which translated to the viral entry assays following the observed trend observed previously for 1.3 and 1.4. However, compound 1.6 has a more lipophilic and basic piperidine group (pK_{a} 9.52) but exhibited reduced potency and selectivity relative to 1.3–1.5. Regardless, these diphyllin derivatives represent potent EBOV entry inhibitors with no observed cytotoxicity in PHM.

Diphyllin and Derivatives Do Not Affect EBOV Association with Cells. The first step of virus infection is binding to cells, which for EBOV can occur through several receptor types after which the virus is taken up through endocytosis. GFP-tagged virus-like particles (GFP-VLPs) were used to monitor association with HeLa cells. Virus-like particles, which morphologically resemble the authentic live virus, are entry-competent but lack the virus genome; thus, they are considered noninfectious and appropriate for use in a BSL-2 setting. HeLa cells were pretreated with compound at concentrations near the approximate IC_{50} values seen in the acridine orange assay that show a correlation with the authentic EBOV infection assays. After incubation with GFP-VLPs, cells were fixed, imaged with epifluorescence microscopy (Figure 4A), and counted particles present inside cells (Figure 4B). 5-(*N*-Ethyl-*N*-isopropyl) amiloride (EIPA) is an inhibitor of macropinocytosis, while NH_4Cl alters an endocytic buffering capacity and both serve as controls.⁵⁰ In each case, diphyllin and its derivatives had minimal to no effect on VLP association and

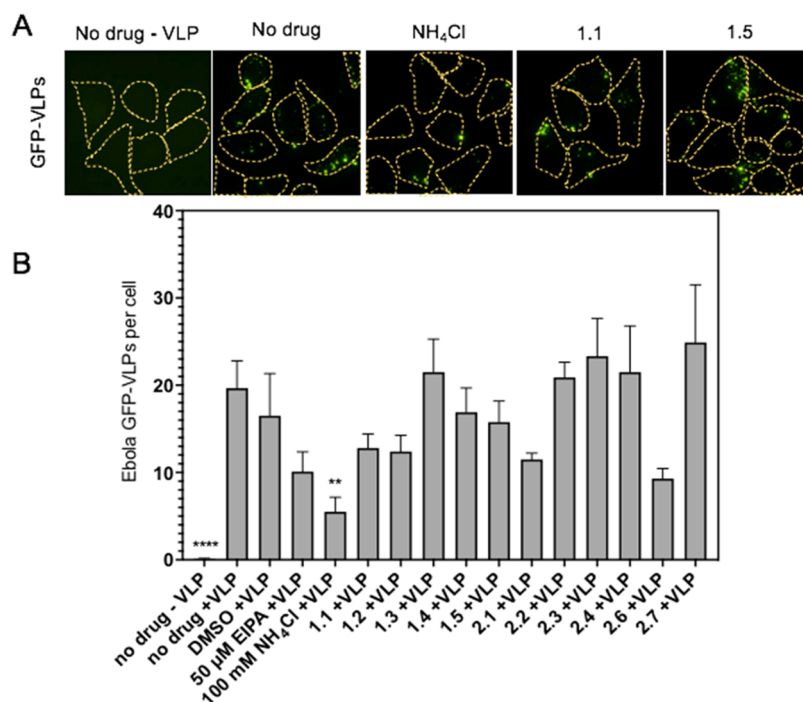


Figure 4. Effect of diphyllin and derivatives on VLP cell binding. (A) Representative images of the Ebola GFP-VLP (green) internalization assay in HeLa cells pretreated with compounds and stained with a cell mask (yellow dotted line) 2 h post-VLP addition. Compounds were dosed at the following concentrations: EIPA at 50 μM, NH₄Cl at 100 mM, diphyllin (1.1) at 500 nM, 1.2–1.3 at 100 nM, 1.5 at 10 nM, 2.1 at 250 nM, 2.2–2.3 at 100 nM, 2.4 at 500 nM, and 2.6 at 250 nM. (B) Quantification of GFP-VLP internalization into cells using CellProfiler software. Statistics represent one-way ANOVA with multiple comparisons to no drug + VLP control.

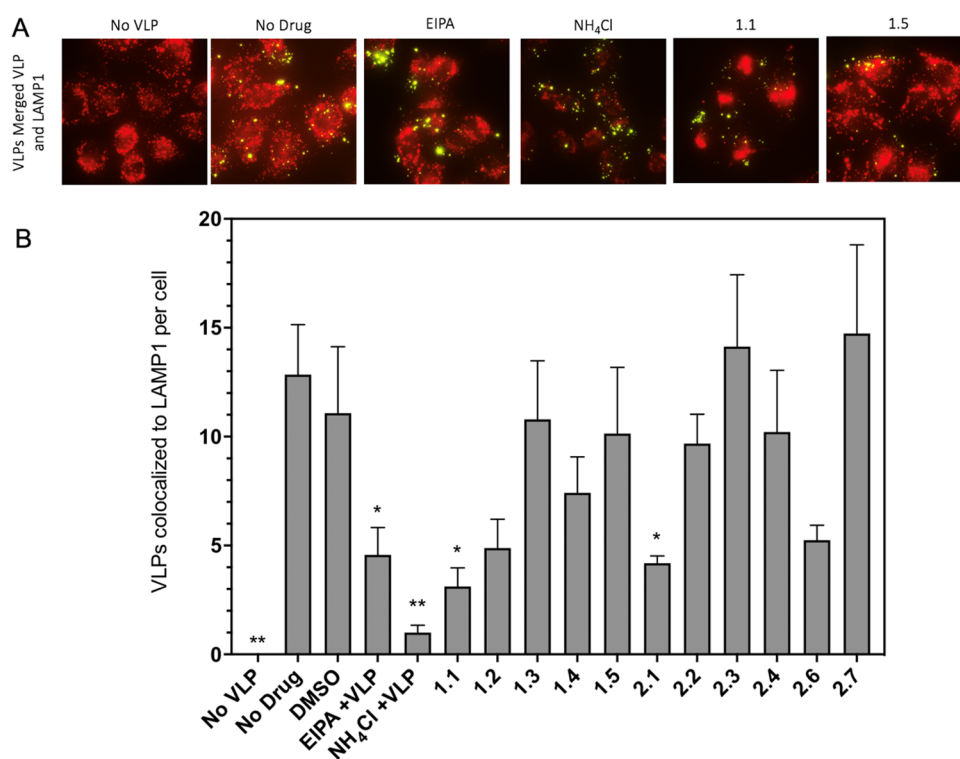


Figure 5. Impact of diphyllin and derivatives on VLP trafficking to lysosomal compartments. (A) Representative images of pretreated HeLa cells infected with GFP-VLPs (green). Two hour post addition, cells were fixed, stained for LAMP1 (red), and imaged with epifluorescent imaging. Compounds were dosed at the following concentrations: NH₄Cl at 100 mM, diphyllin (1.1) at 500 nM, 1.2–1.3 at 100 nM, 1.5 at 10 nM, 2.1 at 250 nM, 2.2–2.3 at 100 nM, 2.4 at 500 nM, and 2.6 at 250 nM. (B) Quantification of the colocalization between GFP-VLPs and LAMP1+ vesicles. Statistics represent a one-way ANOVA with multiple comparisons to the no drug control.

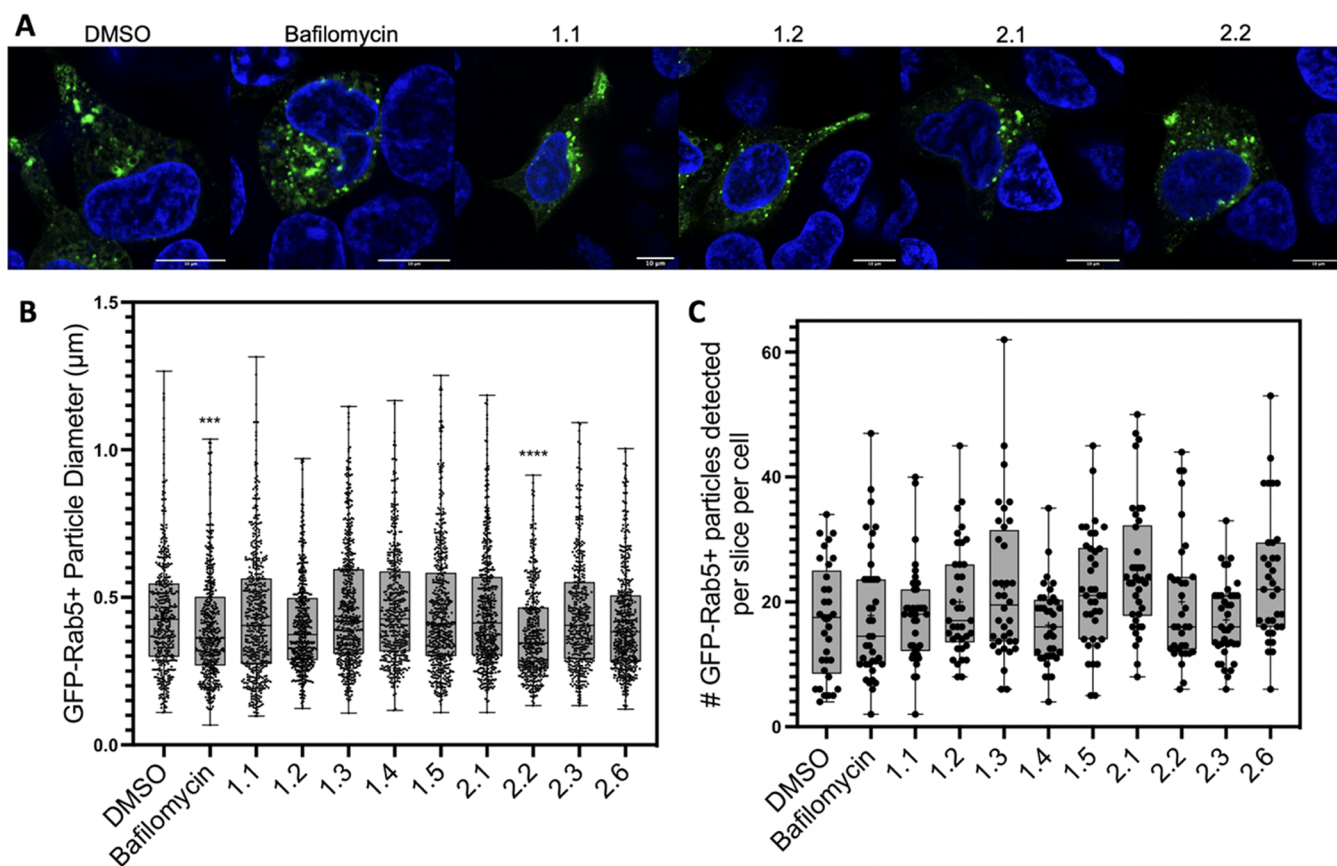


Figure 6. Effect of diphyllin and derivatives on the morphology and population of Rab5+ early endocytic vesicles. (A) Confocal imaging of GFP-Rab5-expressing HEK293 cells treated with drugs for 3 h and stained with Hoechst 33342 nuclear stain. Compounds were dosed at the following concentrations: bafilomycin at 10 nM, diphyllin (1.1) at 500 nM, 1.2–1.3 at 100 nM, 1.5 at 10 nM, 2.1 at 250 nM, 2.2–2.3 at 100 nM, 2.4 at 500 nM, and 2.6 at 250 nM. (B) Quantification of Rab5+ punctate vesicle diameters. Rab5+ vesicles were binned based on their appearance as either punctate or dilated structures. Diameters of vesicles were measured with ImageJ and recorded in Prism 9 software. (C) Quantification of Rab5+ vesicle population. Using ImageJ software, the number of vesicles (punctate and dilated) were counted per cell and analyzed by nested one-way ANOVA with multiple comparisons to DMSO.

uptake in most cases. The results do not correlate with the relative potency of the viral entry inhibition and appear to lack significance.

Diphyllin and Derivatives Show Variable Effects on EBOV-VLP Trafficking to Lysosomes. Since cell association was not affected, subsequent steps leading to cell infection were tested. An early step to EBOV cell entry involves macropinocytosis of the viral particle followed by trafficking through the endocytic pathway.³ Many reported viral entry inhibitors are sufficiently lipophilic agents containing basic nitrogen groups that can accumulate in lysosomes and disrupt organelle functions.^{34,51} Also, NH_4Cl is a known pH disruptor of the endosome–lysosome function while impacting the trafficking of filoviral particles.

A colocalization assay of GFP-VLPs with the lysosomal marker LAMP1 was used as an indicator of the successful routing of the particles through the endocytic pathway. HeLa cells pretreated with diphyllin derivatives at the same concentrations used in the uptake assay were exposed to GFP-VLPs. Cells were fixed and stained for LAMP1 before imaging and quantifying LAMP1 and GFP-VLP colocalization (Figure 5A,B). EIPA and NH_4Cl are known to act at different steps of the uptake and trafficking process, and both agents exhibited inhibition of GFP-VLP association with LAMP1⁺ compartments (EIPA $p = 0.0189$, NH_4Cl $p = 0.0031$). Diphyllin 1.1 at 500 nM

also showed a significant reduction of GFP-VLPs in LAMP1 vesicles, while the more lipophilic 1.2 showed a reduced capacity to inhibit the same colocalization. Surprisingly, the most basic compounds 1.3–1.6 did not inhibit GFP-VLP colocalization with LAMP1. These results argue against a role for a nonspecific basic nitrogen effect on lysosomal functions for compounds 1.3–1.6. In contrast, the less potent inhibitor 2.6 showed a moderate effect on GFP-VLP-LAMP1 colocalization perhaps associated with the additional basic site in the side chain. Despite a range of effects for each treatment and LAMP1 colocalization, except for diphyllin, there appears to be little overall correlation between the potency of viral entry inhibitors and the trafficking of the GFP-VLP to lysosomes.

Diphyllin and Derivatives Do Not Morphologically Disrupt the Endocytic System. The diphyllin derivatives exhibited no observable effects on the VLP trafficking to LAMP1⁺ vesicles, likely lysosomes, while still inhibiting EBOV entry. The results inspired evaluation of the impacts of these compounds on the morphology and population of intracellular compartments of the endocytic system. The first study made use of HEK293 cells expressing a GFP-Rab5 marker for early endosomes (Figures 6 and S6). Cells were treated with compounds for 3 h and fixed and stained with Hoechst 33342 before confocal imaging. Images of at least 10 cells per drug

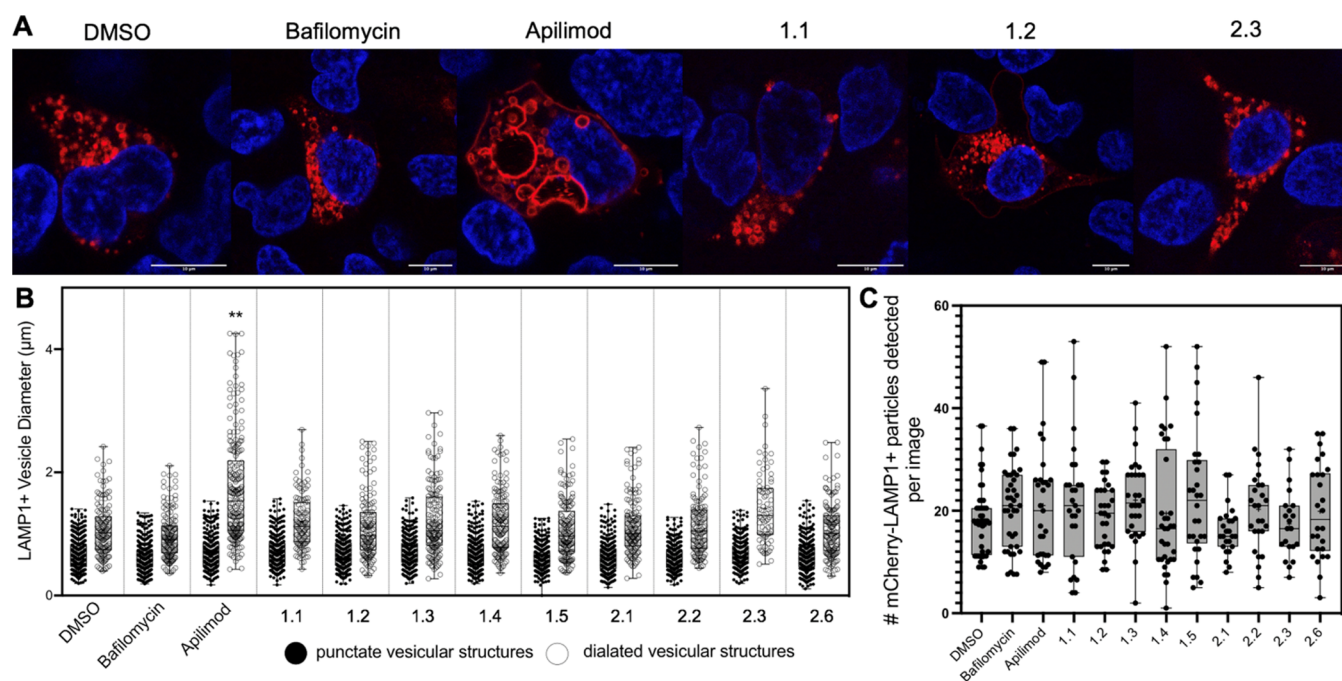


Figure 7. Effect of diphyllyn and derivatives on the morphology and population of LAMP1+ lysosomal vesicles. (A) Confocal imaging of mCherry-LAMP1-expressing HEK293 cells treated with drugs for 3 h and stained with Hoechst 33342 nuclear stain. Compounds were dosed at the following concentrations: bafilomycin at 10 nM, apilimod at 200 nM, diphyllyn (1.1) at 500 nM, 1.2–1.3 at 100 nM, 1.5 at 10 nM, 2.1 at 250 nM, 2.2–2.3 at 100 nM, 2.4 at 500 nM, and 2.6 at 250 nM. (B) Quantification of LAMP1+ lysosome size. LAMP1+ vesicles were binned based on their appearance as either punctate or dilated structures. Diameters of vesicles were measured with ImageJ and recorded in Prism 9 software. (C) Quantification of LAMP1+ vesicle population. Using ImageJ software, the number of vesicles (punctate and dilated) was counted per cell. Statistics reflect a one-way nested ANOVA run with multiple comparisons to DMSO.

condition in each biological replicate were collected, and the number of vesicles in each image was determined.

Vesicles were binned into two groups: punctate and dilated structures. The average size of Rab5⁺ punctate structures in DMSO-treated cells was found to be 450 nm; this is consistent with prior studies which estimate the size of a mature endosome at 500 nm.⁵² Bafilomycin treatment showed a moderate reduction in the size of Rab5⁺ vesicles, with an average of 400 nm. Like bafilomycin, compound 2.2 also induces a significant reduction in the size of Rab5⁺ vesicles to an average of 380 nm. Surprisingly, all of the other diphyllyn derivatives tested, including 1.1–1.5, 2.1, 2.3, and 2.6, showed minimal to no effect on the sizes of Rab5⁺ vesicles, with averages between 410 and 460 nm.

The second study used mCherry-LAMP-1 as a marker for endolysosomes in HEK293 cells (Figure 7). This experiment also used the known PIKfyve inhibitor apilimod, previously shown to block EBOV viral entry, as a positive control.⁵³ Apilimod-treated cells were the only case with any significantly altered LAMP1⁺ structures compared to the DMSO vehicle. Dilated LAMP1⁺ structures became distinct as enlarged and coalescing compartments.⁵⁴ However, the punctate structures were not significantly affected. In all other compound treatments, perturbation of the LAMP1⁺ puncta and dilated vesicle structures was not observed.

Diphyllyn and Derivatives Can Block and Reverse Apilimod-Induced Lysosomal Coalescence. Bafilomycin has been shown to reverse the endolysosome dilation induced by the drug apilimod.⁵⁵ If V-ATPase inhibition is a mechanism for this reversal, the diphyllyn derivatives would be expected to have an impact on the dilated compartments. The first study was designed to test the ability of diphyllyn derivatives to block the

formation of apilimod-induced large compartments in HEK293 cells expressing mCherry-LAMP1. Following inhibitor pretreatments, the cells were challenged with apilimod, stained with nuclear stain, and imaged by confocal microscopy (Figure 8A). The numbers of large (>1 μm) dilated vesicles per cell were determined (Figure 8C).

In cells pretreated with DMSO, there was an average of 8 dilated vesicles >1 μm per cell. The average dropped to nearly 1 in cells pretreated with bafilomycin, which is known to block apilimod's lysosomal phenotype. Similarly, treatment with diphyllyn derivatives significantly decreased the number of large, dilated vesicles in apilimod-treated cells.

The second study assessed the ability of diphyllyn derivatives to reverse an established apilimod-induced phenotype. Apilimod pretreated cells were challenged with the DMSO vehicle, bafilomycin, or diphyllyn derivatives. Cells were stained and imaged with confocal microscopy following the second treatment (Figure 8B,D). In apilimod-treated cells with DMSO controls, there was an average of eight large, dilated vesicles per cell. This average significantly dropped to nearly 1 in cells treated with bafilomycin. Similarly, diphyllyn and derivatives significantly decreased the number of large, dilated vesicles in apilimod-treated cells.

Finally, a third study was performed to evaluate whether diphyllyn derivatives could reverse the phenotype of the constitutively active (CA) Rab5 mutant Q79L. This mutation causes enlarged dilated Rab5⁺ compartments that phenocopy the effects of apilimod on endolysosomes. A prior report connecting the Q79L mutation and bafilomycin-induced effects on vacuolation of early endosomes implicates a role for V-ATPase.⁵⁶ The diphyllyn derivatives were used to test whether V-ATPase inhibition impacts the dilated phenotype. HEK293

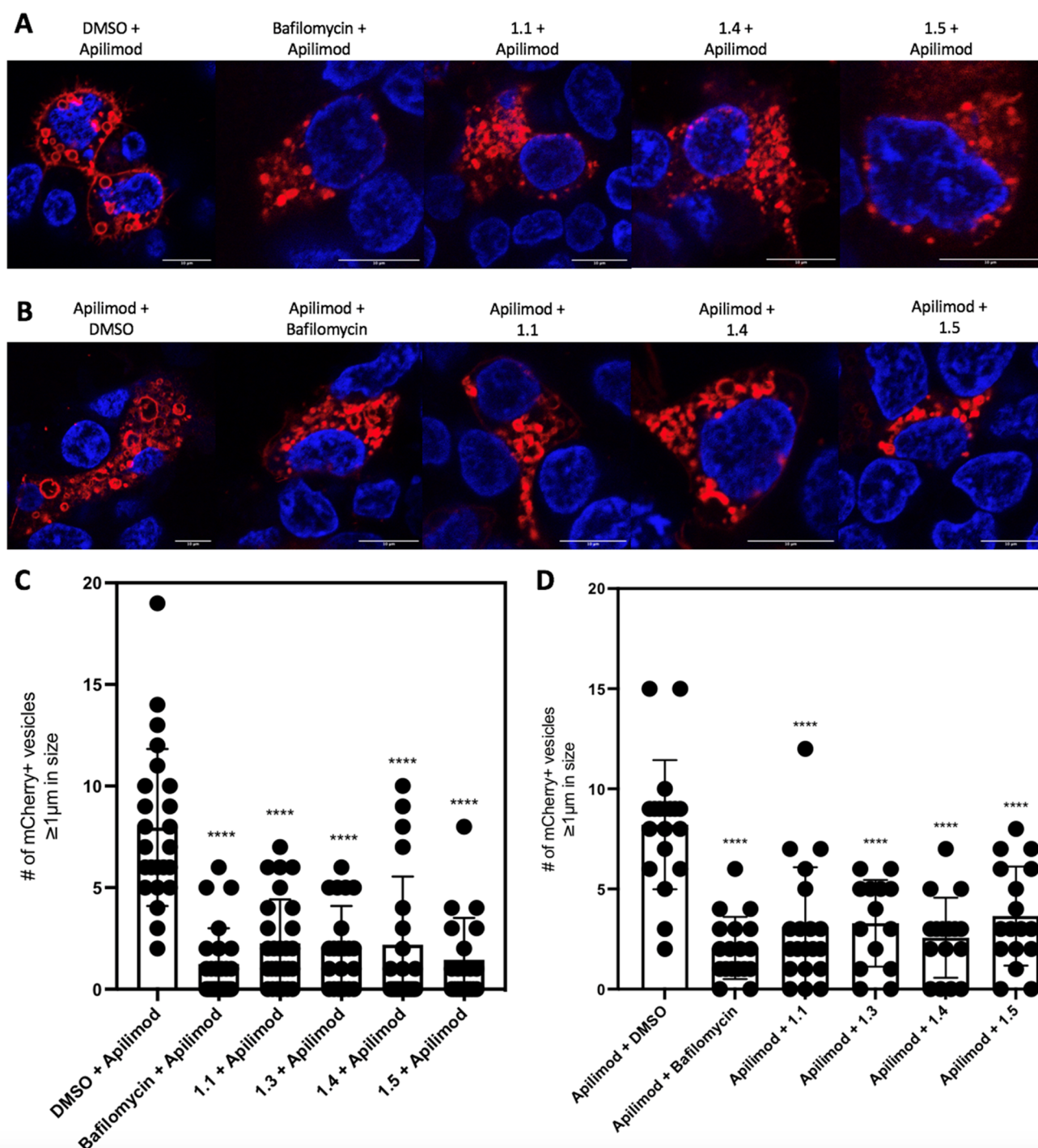


Figure 8. Blockage and reversal of apilimod-induced LAMP1 lysosomal coalescence phenotype by diphyllin and derivatives. (A) Representative images of mCherry-LAMP1-expressing HEK293 cells treated with 500 nM diphyllin and 100 nM derivatives (1.2–1.5) for 1 h followed by a 1 h 200 nM apilimod treatment. (B) Representative images of mCherry-LAMP1-expressing cells treated with apilimod for 1 h followed by a 1 h treatment with diphyllin and derivatives. (C) Quantification of the number of dilated mCherry+ vesicles $>1 \mu\text{M}$ in size when mCherry-LAMP1-expressing HEK293 cells were treated with diphyllin and derivatives for 1 h followed by a 1 h apilimod treatment. (D) Quantification of the number of dilated mCherry+ vesicles $>1 \mu\text{M}$ in size when mCherry-LAMP1-expressing HEK293 cells were treated with apilimod for 1 h followed by a 1 h treatment with diphyllin and derivatives. Statistics represent a one-way ANOVA with multiple comparisons to DMSO.

cells expressing GFP-Rab5 CA Q79L were used to test this hypothesis (Figure S7A). The number of large ($>1 \mu\text{m}$) dilated vesicles were counted (Figure S7B). Strikingly, V-ATPase inhibitors did abrogate the Rab5 CA Q79L phenotype: DMSO-treated cells had an average of three enlarged vesicles. In contrast, bafilomycin had an average of 1.3, diphyllin (1.1) an

average of 1.5, and for compounds 1.3–1.5, there was a range of averages from 0.9 to 1.2.

Diphyllin and Derivatives Have a Reversible Effect on the pH of Endocytic Vesicles. While diphyllin and derivatives were all able to prevent the pH-dependent accumulation of acridine orange in endosomes, the dynamics of the effects are

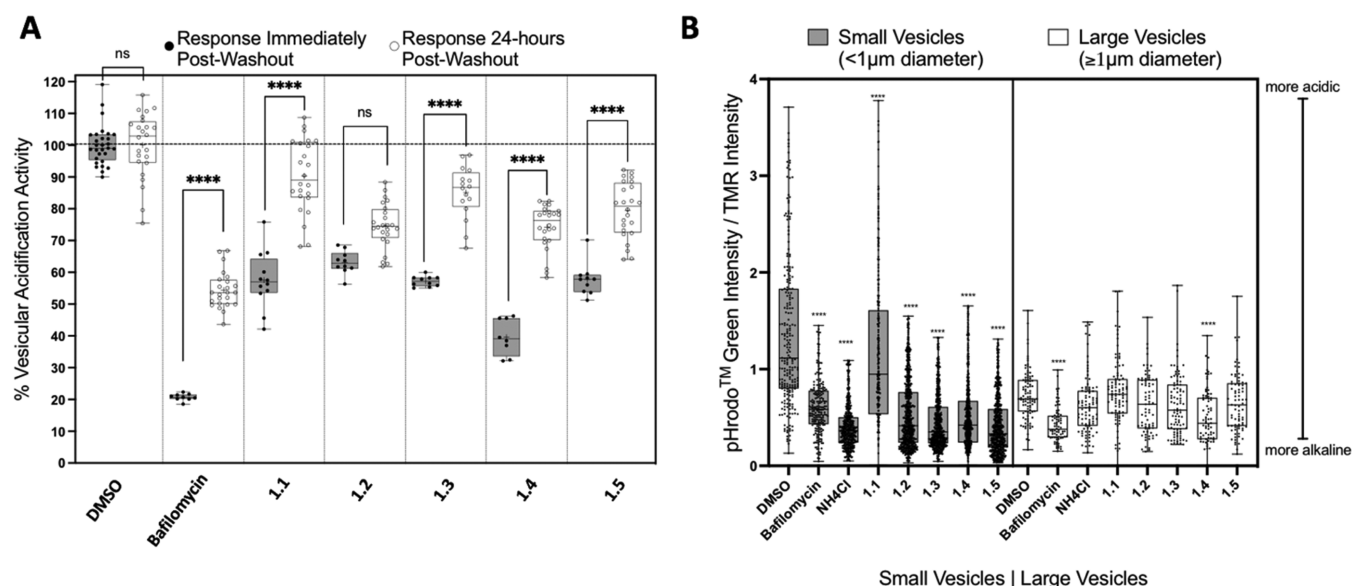


Figure 9. Reversibility of diphyllin and derivatives on endocytic pH. (A) HEK293 cells were treated with compounds for 3 h. Bafilomycin was dosed at 10 nM, diphyllin (1.1) at 500 nM, 1.2–1.4 at 100 nM, and 1.5 at 10 nM. Subsequently, cells were washed with phosphate-buffered saline and either loaded with acridine orange and read for the immediate post washout response or incubated in Opti-MEM media for an additional 24 h before loading and reading the 24 h post washout response. (B) Diphyllin and derivatives tested on the dual uptake assay. HEK293 cells pretreated with compounds for 1 h were loaded with a pH-sensitive probe (pHrodo Green Dextran 10 kDa) and a pH-insensitive probe (TMR-Dextran 10 kDa). Bafilomycin was dosed at 10 nM, diphyllin (1.1) at 500 nM, NH₄Cl at 40 mM, and all diphyllin analogues (1.2–1.5) at 100 nM. Twenty minutes after loading with the dyes, cells were stained with nuclear stain and imaged with live-cell confocal microscopy. CellProfiler software was used to identify stained vesicular structures and calculate the ratio of fluorescence intensities of the pH-sensitive dye to pH-insensitive dye. Structures were binned into small and large bins based on their size. Statistics represent a one-way ANOVA with multiple comparisons to the DMSO control for each bin.

not clear. Since diphyllin was found to be significantly less toxic to cells than bafilomycin, the potential for reversible effects on endosome pH was assessed using the same acridine orange assay. The reversibility assay was performed by treating cells with compounds for 3 h, before removal by washing, and loading with acridine orange to determine the immediate response. The second set of cells were put into Opti-MEM serum-free media for 24 h before loading with acridine orange and evaluating the response post washout. Acridine orange is a dichromatic cell-permeable fluorescent dye that makes a metachromatic shift from green to red when trapped in acidic vesicular organelles like endosomes and lysosomes. In these acidic compartments, acridine orange is protonated and no longer permeable to cellular membranes.

When normalized with the DMSO-treated cells, the % response can be interpreted as the percent of endogenous vesicular acidification activity. There was no significant difference between the vesicular acidification activity in cells before and 24 h post washout for the DMSO control treatment. However, the inhibition of vesicular acidification was reversible to differing degrees with bafilomycin, diphyllin, and derivatives (Figure 9A). Bafilomycin shows the highest percent inhibition, but the full recovery of acridine orange pH-dependent shift to red was not observed. In contrast, diphyllin-treated cells (1.1) returned from an initial response of $57.5 \pm 9.0\%$ acidification activity to $90.2 \pm 11.5\%$ activity after the 24 h washout period. Likewise, the effects of compounds bearing a nitrogen heterocycle including 1.3–1.5, 2.2, 2.4, 2.6, and 2.7 were all reversible and, in many cases, exceeded diphyllin (Figures 9A and S8). Interestingly, recovery of vesicular acidification activity from derivatives 2.1 (95.3%) and 2.3 (97.0%) was not complete. Finally, cells treated with compound 1.2 bearing a simple alkyl

side chain showed a contrasting weak recovery in acidification activity that was not statistically significant (p 0.0764).

However, there is the potential for unknown assay interferences by the diphyllin derivatives despite the non-overlapping excitation and emission spectral properties. The pH-dependent endocytic effects observed in HEK293 cells were evaluated using a second assay to assess the subcellular compartment pH effects of diphyllin and derivatives using the dual dextran uptake assay. The pH-sensitive dye, pHrodo, was used to assess the pH of dextran-loaded endocytic vesicles; the pH-insensitive dye, TMR, was used to assess proper dextran uptake into the endocytic system. The effects measured on the pH-sensitive dye (pHrodo) can be normalized to those measured on the pH-insensitive dye (TMR) to account for changes in dextran loading after compound treatments. Cells were pretreated with compounds for 1 h before loading with 0.1 mg/mL pHrodo-dextran 10 kDa and 1 mg/mL TMR-dextran 10 kDa. Cell images were split into the red (TMR) and green (pHrodo) channels with background subtracted. The ratio of green to red intensities was calculated for each object before binning based on size: objects $\geq 1 \mu\text{m}$ in diameter and $< 1 \mu\text{m}$ in diameter (Figure 9B). Diphyllin derivatives significantly ($p < 0.0001$) decrease the amount of pHrodo fluorescence in small ($< 1 \mu\text{m}$) TMR-loaded vesicles consistent with an increase of pH. The characteristics of the larger ($> 1 \mu\text{m}$) vesicle populations were not clear. However, the apparent pH of these compartments was overall more alkaline and far less sensitive to the effects of NH₄Cl. A significant decrease ($p < 0.0001$) in the large vesicle pHrodo fluorescence was only observed with bafilomycin and 1.4-treated cells.

Structural Features Modulate Cellular Selectivity of the Diphyllin Scaffold Distinct from Bafilomycin. These results implicate the diphyllin scaffold as a core pharmacophore

and highlight a critical role of the ether linkage to nitrogen substitutions in cellular targeting to establish potency and selectivity. Natural derivatives of diphyllin are known that have methyl or glycosyl linkages to the phenol group.⁵⁷ An example is a 6-deoxyglucosyl-diphyllin derivative, which showed *in vivo* efficacy in a Zika infection model.⁴⁰ However, adding glycosyl groups can enhance activities associated with cytotoxic effects.⁵⁸ The case of compounds 1.3–1.6 highlights a different substitution type using nitrogen-containing heterocycles that affect greater potency as inhibitors of EBOV cell entry over the parent diphyllin. These groups appear to provide >100-fold selective compounds improving viability as host targeted antiviral agents. Even in the analogues where the viral entry inhibition potency is reduced, there remains a high degree of selectivity. Interestingly, the inhibitor potencies using isolated vesicle V-ATPase do not all correlate well with cellular activities. The physicochemical properties of the nitrogen heterocycle in localizing the diphyllin core to the vesicle compartments containing V-ATPase maybe a key feature to enhance potency. A related study revealed a similar property-based morpholino group linked through a phenol ether that targets the V0 domain of V-ATPase.⁵⁹ Potential for further optimization will need to find a balance that ensures cellular localization with the target.

Effects of Diphyllin Derivatives Are Distinct. The lack of impact of the diphyllin derivatives on vesicle trafficking is consistent with the results of VLPs reaching the endolysosomes in the presence of the compounds. These results alone do not explain the mechanism of viral entry inhibition. The potency of viral entry inhibition appears related to pH effects on smaller vesicle compartments in the endosome–lysosome pathway. A reasonable hypothesis would be that the pH-dependent viral-membrane fusion step, such as the EBOV GP's cathepsin processing, is impacted. Further studies will be needed to address this potential mechanism of action.

It does appear that the potency of viral entry inhibition correlates with the degree of intracellular vesicle neutralization. These effects are fully reversible with diphyllin and derivatives distinct from bafilomycin, where cells never fully recovered vesicle acidification. Since the two compounds are in very different structural classes, the degree of compound distribution in cellular compartments is likely distinct. The extent to which the reversibility contributes to the reduced cellular toxicity of the diphyllin derivatives relative to bafilomycin is not clear. Another emerging explanation for classifying the particular cellular effects for bafilomycin and diphyllin could be their respective binding in different V-ATPase subunits. The results of these inhibitors on pH in small vesicle compartments are well supported by the data reported here. There were no significant morphological changes to intracellular features observed at the doses of diphyllin derivatives used for these studies consistent with enhanced selectivity of these agents. These results reduce the possibilities that these agents are nonspecific lysosomotropic agents at the doses used to block viral entry. The diphyllin side chains' structural dependence for potency also distinguishes them from the less potent, nontargeted, broad spectrum antiviral effects elicited by amodiaquine, mefloquine, azithromycin, and related classes of drugs.²¹ Importantly, the lack of structural correlations with the basicity or lipophilicity of this series also argues against some type of unrelated lysosomal effects on viral entry. Finally, the fact that the on-target potency does not correlate with the viral entry inhibition implies that the intracellular localization of these agents may be a significant feature for improvement.

METHODS

Plasmid Constructs. The mCherry-Lysosomes-20 plasmid (i.e., LAMP1, Addgene #55073) was a gift from Michael Davidson. The GFP-Rab5B plasmid (Addgene plasmid # 61802) was a gift from Gia Voeltz.⁶⁰ The GFP-Rab5 CAQ79L plasmid (Addgene plasmid # 35140) was a gift from Sergio Grinstein.⁶¹

Cells. HEK293 cells (ATCC CRL-1573) were maintained in Dulbecco's Modified Eagle's medium (DMEM) (Fisher Scientific) supplemented with 10% fetal bovine serum (FBS) (R&D Systems, Minneapolis, MN) (referred to here as complete medium). Caco-2 cells (ATCC HTB-37) were cultured in DMEM supplemented with 10% FBS, 1× penicillin/streptomycin, 1× nonessential amino acids, and 2 mM L-glutamine in T-75 flasks at 37 °C in 5% CO₂ and 90% relative humidity. Cells were grown for at least 2 weeks after removing from cryopreservation before studies were conducted.

Inhibition of Cellular Vesicle Acidification. HEK293 cells were seeded into clear 96-well plates (Falcon) at 10,000 cells/well and allowed to grow for 18–20 h at 37 °C and 5% CO₂ in complete medium. Cells were treated with inhibitors at varying concentrations (<2% DMSO) for 4 h before the addition of 1 μg/mL acridine orange in DMEM for 10 min before media was removed and cells washed twice with 1× phosphate-buffered saline (PBS). Fluorescent readings were taken with a Biotek Synergy 4 microplate reader using the following filter pairings: 485/20–530/30 and 485/20–665/7 nm. Data shown are the 665/530 nm emission ratio for 12 individual experiments. IC₅₀ data are reported as the concentration at which 50% of the 665/530 nm ratio was inhibited relative to the vehicle-treated control with the standard deviation. All compounds were also assayed without the acridine orange dye to determine if background fluorescence was interfering with the assay. This background fluorescence was determined by washing cells with 1× PBS twice and reading in both fluorescence wavelengths and subtracted from the total fluorescence in both channels before determining the fluorescent ratio after dye treatment.

Determination of Cytotoxicity. HEK293 cells were seeded into clear 96-well plates (Falcon) at 10,000 cells/well and allowed to grow for 18–20 h at 37 °C and 5% CO₂ in complete medium until they reached ~80% confluency. Cells were then treated with inhibitors at varying concentrations (<2%DMSO) for 72 h. Then, 0.5 mg/ml MTT was added to cells for 4 h before quenching the reaction with acidic isopropanol (10% Triton, 0.1 M HCl). After incubation for 24 h at room temperature, the absorbance at 570 and 650 nm was measured using a Biotek Synergy 4 microplate reader. The absorbance at 650 nm was subtracted from the 570 nm to normalize data to any residual media fluorescence. Data are shown as mean ± standard error of the mean of the normalized 570 nm absorbance. CC₅₀ data are reported as the concentration at which cell viability was 50% relative to the controls with the standard deviation for 12 individual experiments.

HEK293 Vesicle Isolation. The isolation and assays were performed similarly to that previously described.^{62,63} In brief, cells were grown to confluency with complete medium in a 175 cm² flask (Corning) before growth media was removed and replaced with serum-free DMEM for 2 h. To neutralize endosomes prior to lysis, FCCP was added to the cellular media to reach a final concentration of 1 μM. Cells were incubated with FCCP for 15 min before cells were scrapped

from the plate and pelleted at 1000g for 5 min. The media was discarded and cells were resuspended in HEK assay buffer (20 mM HEPES, 5 mM glucose, 50 mM sucrose, 50 mM KCl, 90 mM potassium gluconate, 1 mM EGTA, Pierce protease inhibitor mini tablet, pH = 7.4) and were then lysed by passage through a 22 gauge needle 10–15 times. Lysates were then centrifuged at 10,000g for 30 s with a Beckman Coulter Microfuge 22R centrifuge. The supernatant was removed and centrifuged at 14,500g for 20 min. The remaining supernatant was discarded, and the pellet was resuspended in HEK assay buffer.

Inhibition of Acridine Orange Quenching Assay. The vesicle mixture was resuspended in HEK assay buffer + 1% bovine serum albumin (BSA) + 6 μ M acridine orange and split into fractions with the protein concentration being 100 μ g/mL and transferred to a clear 96-well plate. The isolated vesicles were pretreated with inhibitors for 1 h at 37 °C. Fluorescent readings were taken with a Biotek Synergy 4 microplate reader with the 485/20 nm excitation filter and the 530/30 nm emission filter. Plates were read at 1 min intervals for 2 min to measure baseline fluorescence before 5 mM ATP and 5 mM MgCl₂ were added to initiate V-ATPase activity. Readings were taken at 1 min intervals for 1 h before the addition of 1 μ g/mL nigericin (Tocris) and further reading for 15 min at 1 min intervals. The change in fluorescence between the 1 h time point after ATP addition and the reading 2 min after nigericin was added were used to quantify the activity of V-ATPase in each sample. Data are shown as mean \pm standard deviation of nine individual experiments for each compound and concentration.

Stability in Cell Media Assessment. Compounds were suspended in DMEM + 10% FBS at 100 mM concentration, and aliquots were removed at 0, 4, 24, 48 h while incubating at 37 °C with 5% CO₂. Sample media was diluted 1/10 in acetonitrile + 0.1% trifluoroacetic acid and cooled to 4 °C for 30 min. Samples were then centrifuged at 14,000g, and the supernatant was removed and analyzed by high-performance liquid chromatography (HPLC) using a Phenomenex Kromasil C18 HPLC column. The percentage of the original sample peak was used to determine the amount of compound remaining at each time point in comparison with phenol standard. Data shown are the mean \pm standard error of the mean for five individual experiments.

Stability in HEK293 Cells. HEK293 cells were seeded into Corning 6-well plates at a concentration of 5×10^5 cells/well in DMEM+10% FBS and incubated overnight at 37 °C with 5% CO₂. The media was then removed and replaced with DMEM +10% FBS containing 100 mM select inhibitors and allowed to incubate for 24 h at 37 °C with 5% CO₂. Media was then collected and cells were washed three times with cold PBS before being allowed to dry for 15 min. A 1:1:0.0005 mixture of acetonitrile:methanol:trifluoroacetic acid was then added to each well and incubated at 4 °C for 16 h. The supernatant was then removed and centrifuged at 14,000g for 10 min to remove cellular debris. The new supernatant was then concentrated to 500 μ L and analyzed by HPLC using Phenomenex Kromasil C18 HPLC column. Data shown are the average of three independent experiments.

GFP-EBOV Virus Infection Assay. Replication competent Zaire Ebola virus (EBOV) Mayinga strain with insertion of GFP between the nucleoprotein (NP) and VP35, which was a kind gift from Heinz Feldmann (NIH, Rocky Mountain Laboratory, Hamilton, MT), was produced in Vero cells. All work was performed in a biosafety level 4 (BSL-4, protection level 4)

laboratory at Boston University.⁶⁴ The virus stock was titered on cells used in assays (HeLa, HEK293 cells) using a focus assay and counting colonies of GFP-expressing cells. For evaluation of small-molecule impact on infection, cells were challenged with a virus dose corresponding to an MOI of 0.1–0.2. Twenty-four hour post infection, cells were fixed with formalin and washed three times with PBS. Nuclei were then stained with Hoeschst 33342 stain (1:10,000 final dilution), and cells were imaged using a Nikon Ti-eclipse microscope and analyzed with CellProfiler. Typically, 5–10,000 cells were evaluated for infection, which at an MOI of 0.2 corresponded over 2000 infected cells for untreated cells. PHMs were similarly treated with compounds at varying concentrations (<1% DMSO) for 1 h and then were infected with GFP-EBOV. IC₅₀ data are reported at the concentration at which 50% of the viral infection was inhibited in comparison to the controls, with the standard deviation for four individual experiments.^{42,64}

Timed Addition Assay. To gauge when treatments were active against virus replication, compounds were added at times after virus addition. HeLa cells were challenged with wild-type EBOV at an MOI of 0.2 and then treated with either diphyllin, 1.5, or hydroxychloroquine either 1 h prior to infection and then at 2, 6, or 18 h post infection. All groups, including untreated controls, were incubated for 48 h before the supernatant was collected for quantitative real-time polymerase chain reaction (qRT-PCR) analysis to measure virus yield, and monolayers were fixed in 10% formalin for staining of viral glycoprotein (GP) as a measure of virus replication. Since wild-type virus was used, replication was measured by GP levels in cells. For staining of viral GP, plates were removed from formalin and washed three times with PBS. Staining of EBOV GP was done using a primary antibody (Mouse Anti-EBOV, 4F3, IBT Bioservices, Cat. #0201-020) followed by a secondary Alexa 546-conjugated goat anti-mouse antibody (Thermo, Cat. #A-21123). Nuclei were stained using Hoechst 33342 (1:10,000 final dilution). Plates were imaged on a Cytation automated imager, and infection and nuclei counts were measured using Cell Profiler software. For qRT-PCR, virus particles in culture supernatants were lysed in 0.1% Triton X-100 detergent containing buffer supplemented with RNase inhibitor as described elsewhere.⁶⁵ qPCR was conducted according to the NEB Luna Universal qRT-PCR kit (Cat. # E3006L) using CDC-developed primer sets purchased from IDT. GraphPad Prism was used for graphical and statistical analysis.

Production of EBOV GFP-VLPs. EBOV VLPs were produced as previously described.⁶⁴ Briefly, VLPs were produced by calcium phosphate cotransfection of four plasmids encoding Ebola proteins VP40, NP, GP, and GFP-VP40 into HEK293FT cells. VLPs were harvested from cell culture media 48 h after transfection. Cultured media was clarified by centrifugation at 1800g for 15 min. The clarified media was overlaid on a 20 mM HEPES buffered 20% (w/v) sucrose cushion and concentrated by ultracentrifugation at 141,118g for 2 h. VLPs were resuspended in Dulbecco's PBS, stored in small aliquots and frozen in liquid nitrogen prior to storage at –80 °C. VLPs were thawed only once, immediately prior to use.

GFP-VLP Uptake and Trafficking Assays. HeLa cells were seeded into eight well Ibidi slides (cat. no. 80826; Ibidi, Madison, WI) at a concentration of 20,000 cells per well and incubated overnight prior to VLP entry studies. Compounds tested were diluted into DMEM media containing 2% fetal bovine serum (<0.15% DMSO). Cells were treated with the compound of interest for 1 h prior to removal of used media and

replenishing with 200 μL of fresh media containing 10 μL of VLP suspension and the same concentration of test compound. Cells were incubated for 2 h prior to quickly rinsing three times with 200 μL of cold Dulbecco's PBS. Each well was filled with 200 μL of cold PBS buffered 10% formalin and stored at 4 °C overnight until imaged on the epifluorescent microscope. As a control, 100 mM NH_4Cl (cat. no. A661, Fisher, Grand Island, NY) was included.

Immunofluorescence Staining and Image Analysis.

Wells were washed three times in Dulbecco's PBS and permeabilized for 10 min with 0.1% Triton X-100 (cat. no. 9002-93-1, Fisher, Grand Island, NY). Samples were blocked for 30 min at room temperature with 5% v/v goat serum (cat. no. ICN19135680, Life Technologies, Carlsbad, CA) in Dulbecco's PBS (DPBS). Primary anti-LAMP1 antibody (cat no. ab24170, Abcam) and Alexa-546 conjugated goat anti-Rabbit secondary antibody (ThermoFisher, A11035) were used to visualize LAMP1. Cell Mask Blue (ThermoFisher, cat no. H32720) was used at a 1:10,000 dilution in DPBS to visualize the cell body. Fluorescence images of three channels, green (GFP, 488 nm), orange (Alexa 546, 546 nm), and UV (Cell Mask, 350 nm) were used to visualize VLPs and cells. Ten fields of view were used to capture immunofluorescence image stacks for each sample using a Nikon Ti-Eclipse microscope (Nikon, Melville, NY). Z-stack images were converted to maximum intensity projections (MIPs) and split into their corresponding channels using Fiji ImageJ. Colocalization was quantified using the overlapping object tool on CellProfiler. Graphpad Prism was used for ANOVA analyses.

Endosome and Lysosome Morphology and Population Assays. HEK293 cells were seeded in 35 mm glass-bottom dishes (Fisher Scientific) for a confluency of approximately 70% at the time of transfection. For early endosome morphology and population experiments, a transfection mixture of 1 μg of GFP-Rab5 (Addgene # 61802), 7.5 μL of Mirus transfection reagent TransIT LT1, and 250 μL of Opti-MEM was used. For lysosome morphology and population experiments, a transfection mixture of 750 ng of mCherry-Lysosomes-20 (Addgene plasmid #55073), 7.5 μL of Mirus transfection reagent TransIT LT1, and 100 μL of Opti-MEM was used. The morning following the transfection, cells were switched into DMEM+10% FBS and drugged accordingly with a final DMSO concentration of 0.15%. Drugs were incubated with cells for 3 h at 37 °C, 5% CO_2 . Hoechst 33342 nuclear stain diluted in PBS was added to cells for a final concentration of 1:10,000 and incubated for the final 20 min of drug treatment. After treatment, cells were fixed in 1 mL 4% PFA for 10 min at room temperature followed by washing with ice-cold PBS. Fixed samples were stored in PBS at 4 °C until imaging. Three biological replicates were performed on different days.

Analysis of Endosome and Lysosome Morphology.

Images were collected as described in the confocal imaging [Methods](#) section. To analyze the morphology of endocytic vesicles, Rab5⁺ or LAMP1⁺ vesicle sizes (diameters) were measured using the straight edge line tool in FIJI. For each experiment, vesicles were binned into two bins: punctate vesicular structures or dilated (defined by a dark hole visible in the center) vesicular structures. Diameters were recorded in Prism 8 software. Data points collected in a nested column data table were cleaned by identifying outliers using the ROUT method, performing the calculation for each subcolumn separately with a $Q = 0.1\%$ (removes definitive outliers). Data for both punctate and swollen dilated vesicular structures were

analyzed using a nested one-way ANOVA with multiple comparisons to the DMSO control.

Analysis of Endosome and Lysosome Populations.

Images were collected as described in the confocal imaging [Methods](#) section. ImageJ software was used to threshold, remove noise, and count the number of particles in the image with an area $>0.05 \mu\text{m}^2$. For both Rab5 and LAMP1 vesicles, data points collected in a column data table were cleaned by identifying outliers using the ROUT method, performing the calculation with a $Q = 1\%$. A nested one-way ANOVA was run with Dunnett's multiple comparison test.

Dual Dextran Uptake Endolysosomal pH Assay.

HEK293 cells were seeded in four-chamber 35 mm glass-bottom dishes (Cellvis) for 70% confluency on the day of the experiment. Drugs were incubated with cells for 1 h, and then cells were loaded with 0.1 mg/mL pHrodo-dextran 10 kDa (Thermo Scientific) and 1 mg/mL TMR-dextran 10 kDa (ThermoFisher Scientific) and costained with Hoechst 33342 nuclear stain for 20 min at 37 °C. After dextran loading and staining, cells were imaged with confocal microscopy. Drug effect on pH was quantified using the intensity of pHrodo normalized to the intensity of TMR per vesicle. Data was binned based on vesicle size: either $>$ or $<1 \mu\text{m}$ in diameter. CellProfiler was used to quantify the images. Prism 8 was used to graph and analyze the data with one-way ANOVA with multiple comparisons to the DMSO control for each bin.

Reversibility of V-ATPase Inhibition in Acridine Orange Response.

HEK293 cells were seeded into 96-well black, glass-bottom plates, and drug treatments began when cells were 90% confluent. Drugs were diluted in DMEM + 10% FBS to be at or near their IC_{50} with a final DMSO concentration of 0.15%; 100 μL of drugged media was placed into the appropriate wells. Cells were incubated with drugs for 3 h at 37 °C, 5% CO_2 . After treatment, drugged media was aspirated. Plates used to collect AO response immediately post washout were washed with Opti-MEM and then incubated with 100 μL 1 $\mu\text{g}/\text{mL}$ acridine orange in PBS for 20 min at 37 °C, 5% CO_2 ; subsequently, cells were washed with PBS + 3% FBS and then had fluorescent readings taken with Molecular Devices SpectraMax M5e using the following filter pairings: 485/20–530/30 and 485/20–665/7 nm. Plates used to collect washout AO response were washed thoroughly after drug treatment and incubated in 100 $\mu\text{L}/\text{well}$ of Opti-MEM for 24 h at 37 °C, 5% CO_2 ; at this point, Opti-MEM was aspirated and the acridine orange assay was run and fluorescence measured using the same protocol as the immediate post washout plates. The 665/530 nm emission ratio was calculated for each well and input into Prism 8. Ratios of treatment wells were normalized to the average of the technical replicates of DMSO on the same plate, with DMSO as 100% endogenous vesicular acidification activity (equation used: $(1 - ((\text{DMSO-Drug})/\text{DMSO})) \times 100\%$). The normalized data were cleaned using the ROUT method with a $Q = 1\%$. Cleaned data were compiled into a grouped table that was used to run a two-way ANOVA and Sidak's multiple comparisons test run by comparing cell means regardless of rows and columns and by comparing each cell mean with every other cell mean. Ordinary one-way ANOVA with Dunnett's multiple comparisons to Diphyllin was run on the cleaned normalized 24 h washout data to determine if the derivatives had significantly different reversibility.

Reversibility of Rab5 Constitutively Active Mutant Q79L Phenotype. HEK293 cells were seeded in the wells of a black, glass-bottom 6-well plate (Cellvis) for a confluency of

approximately 70% at the time of transfection. Using the calcium phosphate transfection methods provided by Abcam, 1 μg of GFP-Rab5 CA Q79L (Addgene plasmid # 35140) was transfected into cells overnight. The following morning, media was changed to fresh DMEM + 10% FBS and drugs were added with a final DMSO concentration of 0.15%. Drugs were incubated with cells for 1 h, and then, cells were fixed, stained, and imaged with confocal microscopy. At least five cells were analyzed per biological replicate. Three biological replicates were performed. Images were collected as described in the confocal imaging [Methods](#) section and analyzed in ImageJ software. Rab5⁺ vesicles were measured and manually counted and were recorded in a column table in Prism 8 software. A nested one-way ANOVA was run with Dunnett's multiple comparison test to determine statistical significance.

Inhibition of Apilimod-Induced Lysosomal Phenotypes. HEK293 cells were seeded in the wells of a black, glass-bottom 6-well plate (Cellvis) for a confluency of approximately 70% at the time of transfection. Using the calcium phosphate transfection methods provided by Abcam, 1 μg of mCherry-Lysosomes-20 (Addgene plasmid #55073) was transfected into cells overnight. The following morning, media was changed to fresh DMEM + 10% FBS and drugs were added with a final DMSO concentration of 0.15%. Drugs were incubated with cells for 1 h, and then, apilimod was added for a final concentration of 200 nM and incubated for 30 min–1 h. Cells were then fixed, stained, and imaged with confocal microscopy. At least five cells were analyzed per biological replicate. Three biological replicates were performed on different days. Images were collected as described in the confocal imaging [Methods](#) section and analyzed in ImageJ software. Rab5⁺ vesicles were measured and manually counted and were recorded in a column table in Prism 8 software. A nested one-way ANOVA was run with Dunnett's multiple comparison test to determine statistical significance.

Reversibility of Apilimod-Induced Lysosomal Phenotypes. HEK293 cells were seeded in the wells of a black, glass-bottom 6-well plate (Cellvis) for a confluency of approximately 70% at the time of transfection. Using the calcium phosphate transfection methods provided by Abcam, 1 μg of mCherry-Lysosomes-20 (Addgene plasmid #55073) was transfected into cells overnight. The following morning, media was changed to fresh DMEM + 10% FBS and apilimod was added for a final concentration of 200 nM and incubated for 1 h. Drugs were then added with a final DMSO concentration of 0.15% and incubated for 1 h. Cells were then stained, fixed, and imaged with confocal microscopy. At least five cells were analyzed per biological replicate. Three biological replicates were performed on different days. Images were collected as described in the confocal imaging [Methods](#) section and analyzed in ImageJ software. Rab5⁺ vesicles were measured and manually counted and were recorded in a column table in Prism 8 software. A nested one-way ANOVA was run with Dunnett's multiple comparison test to determine statistical significance.

Confocal Imaging. All confocal imaging was done using the Purdue RHPH Nikon Eclipse Ti A1 instrument using NIS-elements AR software to capture 1024 \times 1024 pixel resolution images at 1/4 frame/second on 60 \times and 100 \times oil objectives detecting the fluorophores with channel series. Nuclear stain in all applicable experiments was captured using Hoechst 33258 laser presets. GFP-tagged proteins were captured using the eGFP laser presets in all applicable experiments. mCherry-tagged proteins were captured using the mCherry laser presets in

all applicable experiments. mCherry-tagged proteins were captured using the mCherry laser presets in all applicable experiments. Following imaging, .nd2 files saved from the microscope were opened in ImageJ and had the background subtracted using a rolling ball radius of 50.0 pixels and contrast enhanced by <0.3% without normalization or equalization of the histogram. The 16 bit image was then converted into RGB color, where it was saved as a tiff with a scale bar.

■ ASSOCIATED CONTENT

Supporting Information

The Supporting Information is available free of charge at <https://pubs.acs.org/doi/10.1021/acsinfecdis.1c00474>.

Inhibition of EBOV entry to HEK293 cells (Table S1); inhibition of the V-ATPase-mediated proton translocation dose–response curve (Figure S1); graphs of selectivity indices (CC50/IC50) (Figure S2); correlations of inhibitor activities (Figure S3); diphyllin and derivative stabilities (Figure S4); chromatographs of isolated inhibitors (Figure S5); effects on morphology of dilated Rab5⁺ endocytic vesicles (Figure S6); reverse of a constitutively active Rab5 mutant Q79L phenotype (Figure S7); reversibility of pH effect (Figure S8); experimental methods; and chemical analysis data (PDF)

■ AUTHOR INFORMATION

Corresponding Author

V. Jo Davisson – Department of Medicinal Chemistry and Molecular Pharmacology, Purdue University, West Lafayette, Indiana 47907, United States; orcid.org/0000-0003-1182-0007; Email: davisson@purdue.edu

Authors

Caroline B. Plescia – Department of Medicinal Chemistry and Molecular Pharmacology and The Purdue Institute for Inflammation, Immunology and Infectious Disease, Purdue University, West Lafayette, Indiana 47907, United States

Aaron R. Lindstrom – Department of Medicinal Chemistry and Molecular Pharmacology, Purdue University, West Lafayette, Indiana 47907, United States

Maritza V. Quintero – Department of Biochemistry and Structural Biology, University of Texas Health San Antonio, San Antonio 78229-3900, United States; orcid.org/0000-0001-8879-7867

Patrick Keiser – Department of Microbiology, National Emerging Infectious Diseases Laboratories, Boston University, Boston, Massachusetts 02118, United States

Manu Anantpadma – Department of Microbiology, National Emerging Infectious Diseases Laboratories, Boston University, Boston, Massachusetts 02118, United States; Present Address: National Institute of Allergy and Infectious Diseases, Integrated Research Facility, Fredrick, Maryland 21702, United States. Email: manu.anantpadma@nih.gov

Robert Davey – Department of Microbiology, National Emerging Infectious Diseases Laboratories, Boston University, Boston, Massachusetts 02118, United States

Robert V. Stahelin – Department of Medicinal Chemistry and Molecular Pharmacology and The Purdue Institute for Inflammation, Immunology and Infectious Disease, Purdue University, West Lafayette, Indiana 47907, United States

Complete contact information is available at:

<https://pubs.acs.org/10.1021/acsinfecdis.1c00474>

Author Contributions

[#]C.B.P. and A.R.L. contributed equally to the experimental results presented in this manuscript; C.B.P. designed and conducted cell imaging-based studies; A.R.L. synthesized and characterized all diphyllin derivatives and conducted all primary testing in nonviral challenged cells and isolated vesicles; M.V.Q. conducted cell entry studies with VLP; M.A. and P.K. conducted all EBOV infection testing; R.D., R.V.S., and V.J.D. were involved in experimental design, data evaluation, manuscript preparations, and copy edits.

Funding

Research reported in this publication was supported by the National Institute of Allergy and Infectious Diseases under awards number R01 AI128364 (V.J.D., R.D.) and T32 AI148103 (C.B.P. and R.V.S.). The authors gratefully acknowledge the support of the shared resources for Biomolecular Structure and Analytical Mass Spectrometry from the Purdue Center for Cancer Research, NIH grant P30 CA023168. The content is solely the authors' responsibility and does not necessarily represent the official views of the National Institutes of Health.

Notes

The authors declare no competing financial interest. V.J.D. is co-founder of Amplified Sciences, Inc.

ACKNOWLEDGMENTS

In addition to all of the authors of this manuscript, the authors would also like to acknowledge and thank Dr. Nathan Dissinger for his help in maintaining cells and preparing plasmid DNA. The authors would like to recognize the Pharmacy Live Cell Imaging Facility for the use of facilities to support the imaging data acquisition.

ABBREVIATIONS

EBOV, Ebola virus; V-ATPase, vacuolar ATPase; LAMP1, lysosomal-associated membrane protein 1; TIM-1, T cell immunoglobulin mucin domain-1; GP, glycoprotein; NPC1, Niemann Pick C-type 1; CADs, cationic amphiphilic drugs; PHM, primary human macrophages; GFP-EBOV, recombinant Ebola virus encoding GFP as a marker of infection; VLP, virus-like particle; GFP-VLP, GFP-tagged virus-like particles; EIPA, 5-(*N*-ethyl-*N*-isopropyl) amiloride; DMSO, dimethyl sulfoxide; PIKfyve, 1-phosphatidylinositol 3-phosphate 5-kinase; DMEM, Dulbecco's Modified Eagle's medium; FCCP, trifluoromethoxy carbonylcyanide phenylhydrazone; BSA, bovine serum albumin; FBS, fetal bovine serum; NP, nucleoprotein; VP40, matrix protein; PBS, phosphate-buffered saline; AO, acridine orange; TMR, tetramethylrhodamine; CA, constitutively active

REFERENCES

- (1) Feldmann, H.; Sprecher, A.; Geisbert, T. W. Ebola. *N. Engl. J. Med.* **2020**, *382*, 1832–1842.
- (2) Mulangu, S.; Dodd, L. E.; Davey, R. T.; Tshiani Mbaya, O.; Proschan, M.; Mukadi, D.; Lusakibanza Manzo, M.; Nzolo, D.; Tshomba Oloma, A.; Ibanda, A.; Ali, R.; Coulbaly, S.; Levine, A. C.; Grais, R.; Diaz, J.; Lane, H. C.; Muyembe-Tamfum, J.-J.; PALM Writing Group for the PALM Consortium Study Team. A Randomized, Controlled Trial of Ebola Virus Disease Therapeutics. *N. Engl. J. Med.* **2019**, *381*, 2293–2303.
- (3) Saeed, M. F.; Kolokoltsov, A. A.; Albrecht, T.; Davey, R. A. Cellular Entry of Ebola Virus Involves Uptake by a Macropinocytosis-Like Mechanism and Subsequent Trafficking through Early and Late Endosomes. *PLoS Pathog.* **2010**, *6*, No. e1001110.

- (4) Hunt, C. L.; Kolokoltsov, A. A.; Davey, R. A.; Maury, W. The Tyro3 Receptor Kinase Axl Enhances Macropinocytosis of Zaire Ebola Virus. *J. Virol.* **2011**, *85*, 334–347.
- (5) Kondratowicz, A. S.; Hunt, C. L.; Davey, R. A.; Cherry, S.; Maury, W. J. AMP-Activated Protein Kinase Is Required for the Macropinocytosis of Ebola Virus. *J. Virol.* **2013**, *87*, 746–755.
- (6) Nanbo, A.; Imai, M.; Watanabe, S.; Noda, T.; Takahashi, K.; Neumann, G.; Halfmann, P.; Kawaoka, Y. Ebola Virus Is Internalized into Host Cells via Macropinocytosis in a Viral Glycoprotein-Dependent Manner. *PLoS Pathog.* **2010**, *6*, No. e1001121.
- (7) Dahlmann, F.; Biedenkopf, N.; Babler, A.; Jahnen-Dechent, W.; Karsten, C. B.; Gnirß, K.; Schneider, H.; Wrensch, F.; O'Callaghan, C. A.; Bertram, S.; Herrler, G.; Becker, S.; Pöhlmann, S.; Hofmann-Winkler, H. Analysis of Ebola Virus Entry Into Macrophages. *J. Infect. Dis.* **2015**, *212*, S247–S257.
- (8) Gnirß, K.; Kühl, A.; Karsten, C.; Glowacka, I.; Bertram, S.; Kaup, F.; Hofmann, H.; Pöhlmann, S. Cathepsins B and L Activate Ebola but Not Marburg Virus Glycoproteins for Efficient Entry into Cell Lines and Macrophages Independent of Tmprss2 Expression. *Virology* **2012**, *424*, 3–10.
- (9) Chandran, K.; Sullivan, N. J.; Felbor, U.; Whelan, S. P.; Cunningham, J. M. Endosomal Proteolysis of the Ebola Virus Glycoprotein Is Necessary for Infection. *Science* **2005**, *308*, 1643–1645.
- (10) Fénéant, L.; Wijs, K. M. S.; Nelson, E. A.; White, J. M. An Exploration of Conditions Proposed to Trigger the Ebola Virus Glycoprotein for Fusion. *PLoS One* **2019**, *14*, No. e0219312.
- (11) Miller, E. H.; Obernosterer, G.; Raaben, M.; Herbert, A. S.; Deffieu, M. S.; Krishnan, A.; Ndungo, E.; Sandesara, R. G.; Carette, J. E.; Kuehne, A. I.; Ruthel, G.; Pfeffer, S. R.; Dye, J. M.; Whelan, S. P.; Brummelkamp, T. R.; Chandran, K. Ebola Virus Entry Requires the Host-Programmed Recognition of an Intracellular Receptor. *EMBO J.* **2012**, *31*, 1947–1960.
- (12) Côté, M.; Misasi, J.; Ren, T.; Bruchez, A.; Lee, K.; Filone, C. M.; Hensley, L.; Li, Q.; Ory, D.; Chandran, K.; Cunningham, J. Small Molecule Inhibitors Reveal Niemann-Pick C1 Is Essential for Ebola Virus Infection. *Nature* **2011**, *477*, 344–348.
- (13) Carette, J. E.; Raaben, M.; Wong, A. C.; Herbert, A. S.; Obernosterer, G.; Mulherkar, N.; Kuehne, A. I.; Kranzusch, P. J.; Griffin, A. M.; Ruthel, G.; Cin, P. D.; Dye, J. M.; Whelan, S. P.; Chandran, K.; Brummelkamp, T. R. Ebola Virus Entry Requires the Cholesterol Transporter Niemann-Pick C1. *Nature* **2011**, *477*, 340–343.
- (14) Liu, H.; Tian, Y.; Lee, K.; Krishnan, P.; Wang, M. K.-M.; Whelan, S.; Mevers, E.; Soloveva, V.; Dedic, B.; Liu, X.; Cunningham, J. M. Identification of Potent Ebola Virus Entry Inhibitors with Suitable Properties for in Vivo Studies. *J. Med. Chem.* **2018**, *61*, 6293–6307.
- (15) Sadewasser, A.; Dietzel, E.; Michel, S.; Klüver, M.; Helfer, M.; Thelemann, T.; Klar, R.; Eickmann, M.; Becker, S.; Jaschinski, F. Anti-Niemann Pick C1 Single-Stranded Oligonucleotides with Locked Nucleic Acids Potently Reduce Ebola Virus Infection In Vitro. *Mol. Ther. Nucleic Acids* **2019**, *16*, 686–697.
- (16) Kang, Y.-L.; Chou, Y.; Rothlauf, P. W.; Liu, Z.; Soh, T. K.; Cureton, D.; Case, J. B.; Chen, R. E.; Diamond, M. S.; Whelan, S. P. J.; Kirchhausen, T. Inhibition of PIKfyve Kinase Prevents Infection by Zaire Ebola Virus and SARS-CoV-2. *Proc. Natl. Acad. Sci. U.S.A.* **2020**, *117*, 20803–20813.
- (17) Stewart, C. M.; Dorion, S. S.; Ottenbrite, M. A. F.; LeBlond, N. D.; Smith, T. K. T.; Qiu, S.; Fullerton, M. D.; Kobasa, D.; Côté, M. A. Diacylglycerol Kinase Inhibitor, R-59-022, Blocks Filovirus Internalization in Host Cells. *Viruses* **2019**, *11*, 206.
- (18) Schafer, A.; Xiong, R.; Cooper, L.; Nowar, R.; Lee, H.; Li, Y.; Ramirez, B. E.; Peet, N. P.; Caffrey, M.; Thatcher, G. R. J.; Saphire, E. O.; Cheng, H.; Rong, L. Evidence for Distinct Mechanisms of Small Molecule Inhibitors of Filoviral Entry. *PLoS Pathog.* **2021**, *17*, No. e1009312.
- (19) Galindo, I.; Garaigorta, U.; Lasala, F.; Cuesta-Geijo, M. A.; Bueno, P.; Gil, C.; Delgado, R.; Gastaminza, P.; Alonso, C. Antiviral Drugs Targeting Endosomal Membrane Proteins Inhibit Distant

Animal and Human Pathogenic Viruses. *Antiviral Res.* **2021**, *186*, No. 104990.

(20) Finch, C. L.; Dyall, J.; Xu, S.; Nelson, E. A.; Postnikova, E.; Liang, J. Y.; Zhou, H.; DeWald, L. E.; Thomas, C. J.; Wang, A.; Xu, X.; Hughes, E.; Morris, P. J.; Mirsalis, J. C.; Nguyen, L. H.; Arolfo, M. P.; Koci, B.; Holbrook, M. R.; Hensley, L. E.; Jahrling, P. B.; Schmaljohn, C.; Johansen, L. M.; Olinger, G. G.; Schiffer, J. T.; White, J. M. Formulation, Stability, Pharmacokinetic, and Modeling Studies for Tests of Synergistic Combinations of Orally Available Approved Drugs against Ebola Virus In Vivo. *Microorganisms* **2021**, *9*, 566.

(21) Bai, J. P. F.; Hsu, C.-W. Drug Repurposing for Ebola Virus Disease: Principles of Consideration and the Animal Rule. *J. Pharm. Sci.* **2019**, *108*, 798–806.

(22) Iversen, P. L.; Kane, C. D.; Zeng, X.; Panchal, R. G.; Warren, T. K.; Radoshitzky, S. R.; Kuhn, J. H.; Mudhasani, R. R.; Cooper, C. L.; Shurtleff, A. C.; Nasar, F.; Sunay, M. M.; Duplantier, A. J.; Eaton, B. P.; Zumbun, E. E.; Bixler, S. L.; Martin, S.; Meinig, J. M.; Chiang, C.-Y.; Sanchez-Lockhart, M.; Palacios, G. F.; Kugelman, J. R.; Martins, K. A.; Pitt, M. L.; Crozier, I.; Saunders, D. L. Recent Successes in Therapeutics for Ebola Virus Disease: No Time for Complacency. *Lancet Infect. Dis.* **2020**, *20*, e231–e237.

(23) Salata, C.; Baritussio, A.; Munegato, D.; Calistri, A.; Ha, H. R.; Bigler, L.; Fabris, F.; Parolin, C.; Palù, G.; Mirazimi, A. Amiodarone and Metabolite MDEA Inhibit Ebola Virus Infection by Interfering with the Viral Entry Process. *Pathog. Dis.* **2015**, *73*, No. fiv032.

(24) Mazzon, M.; Ortega-Prieto, A. M.; Imrie, D.; Luft, C.; Hess, L.; Czesno, S.; Grove, J.; Skelton, J. K.; Farleigh, L.; Bugert, J. J.; Wright, E.; Temperton, N.; Angell, R.; Oxenford, S.; Jacobs, M.; Ketteler, R.; Dorner, M.; Marsh, M. Identification of Broad-Spectrum Antiviral Compounds by Targeting Viral Entry. *Viruses* **2019**, *11*, 176.

(25) Selaković, Ž.; Soloveva, V.; Gharaibeh, D. N.; Wells, J.; Šegan, S.; Panchal, R. G.; Šolaja, B. A. Anti-Ebola Activity of Diazachrysen Small Molecules. *ACS Infect. Dis.* **2015**, *1*, 264–271.

(26) Cui, Q.; Cheng, H.; Xiong, R.; Zhang, G.; Du, R.; Anantpadma, M.; Davey, R. A.; Rong, L. Identification of Diaryl-Quinoline Compounds as Entry Inhibitors of Ebola Virus. *Viruses* **2018**, *10*, 678.

(27) Basu, A.; Mills, D. M.; Mitchell, D.; Ndungo, E.; Williams, J. D.; Herbert, A. S.; Dye, J. M.; Moir, D. T.; Chandran, K.; Patterson, J. L.; Rong, L.; Bowlin, T. L. Novel Small Molecule Entry Inhibitors of Ebola Virus. *J. Infect. Dis.* **2015**, *212*, S425–S434.

(28) Cheng, H.; Schafer, A.; Soloveva, V.; Gharaibeh, D.; Kenny, T.; Retterer, C.; Zamani, R.; Bavari, S.; Peet, N. P.; Rong, L. Identification of a Coumarin-Based Antihistamine-like Small Molecule as an Anti-Filoviral Entry Inhibitor. *Antiviral Res.* **2017**, *145*, 24–32.

(29) Madrid, P. B.; Panchal, R. G.; Warren, T. K.; Shurtleff, A. C.; Endsley, A. N.; Green, C. E.; Kolokoltsov, A.; Davey, R.; Manger, I. D.; Gilfillan, L.; Bavari, S.; Tanga, M. J. Evaluation of Ebola Virus Inhibitors for Drug Repurposing. *ACS Infect. Dis.* **2015**, *1*, 317–326.

(30) Ekins, S.; Lingerfelt, M. A.; Comer, J. E.; Freiberg, A. N.; Mirsalis, J. C.; O'Loughlin, K.; Harutyunyan, A.; McFarlane, C.; Green, C. E.; Madrid, P. B. Efficacy of Tilorone Dihydrochloride against Ebola Virus Infection. *Antimicrob. Agents Chemother.* **2018**, *62*, e01711-17.

(31) Selaković, Ž.; Tran, J. P.; Kota, K. P.; Lazić, M.; Retterer, C.; Besh, R.; Panchal, R. G.; Soloveva, V.; Sean, V. A.; Jay, W. B.; Pavić, A.; Verbić, T.; Vasiljević, B.; Kuehl, K.; Duplantier, A. J.; Bavari, S.; Mudhasani, R.; Šolaja, B. A. Second Generation of Diazachrysenes: Protection of Ebola Virus Infected Mice and Mechanism of Action. *Eur. J. Med. Chem.* **2019**, *162*, 32–50.

(32) Sakurai, Y.; Sakakibara, N.; Toyama, M.; Baba, M.; Davey, R. A. Novel Amodiaquine Derivatives Potently Inhibit Ebola Virus Infection. *Antiviral Res.* **2018**, *160*, 175–182.

(33) Gaisina, I. N.; Peet, N. P.; Wong, L.; Schafer, A. M.; Cheng, H.; Anantpadma, M.; Davey, R. A.; Thatcher, G. R. J.; Rong, L. Discovery and Structural Optimization of 4-(Aminomethyl)Benzamides as Potent Entry Inhibitors of Ebola and Marburg Virus Infections. *J. Med. Chem.* **2020**, *63*, 7211–7225.

(34) Gunesch, A. P.; Zapatero-Belinchón, F. J.; Pinkert, L.; Steinmann, E.; Manns, M. P.; Schneider, G.; Pietschmann, T.; Brönstrup, M.; von Hahn, T. Filovirus Antiviral Activity of Cationic

Amphiphilic Drugs Is Associated with Lipophilicity and Ability To Induce Phospholipidosis. *Antimicrob. Agents Chemother.* **2020**, *64*, e00143–20.

(35) Sauvau, A.; Ciccocanti, F.; Colavita, F.; Di Rienzo, M.; Castilletti, C.; Capobianchi, M. R.; Kepp, O.; Zitvogel, L.; Fimia, G. M.; Piacentini, M.; Kroemer, G. On-Target versus off-Target Effects of Drugs Inhibiting the Replication of SARS-CoV-2. *Cell Death Dis.* **2020**, *11*, No. 656.

(36) Bimbo, L. M.; Denisova, O. V.; Mäkilä, E.; Kaasalainen, M.; De Brabander, J. K.; Hirvonen, J.; Salonen, J.; Kakkola, L.; Kainov, D.; Santos, H. A. Inhibition of Influenza A Virus Infection in Vitro by Saliphenylhalamide-Loaded Porous Silicon Nanoparticles. *ACS Nano* **2013**, *7*, 6884–6893.

(37) Denisova, O. V.; Kakkola, L.; Feng, L.; Stenman, J.; Nagaraj, A.; Lampe, J.; Yadav, B.; Aittokallio, T.; Kaukinen, P.; Ahola, T.; Kuivaniemi, S.; Vapalahti, O.; Kantele, A.; Tynell, J.; Julkunen, I.; Kallio-Kokko, H.; Paavilainen, H.; Hukkanen, V.; Elliott, R. M.; Brabander, J. K. D.; Saelens, X.; Kainov, D. E. Obatoclox, Saliphenylhalamide, and Gemcitabine Inhibit Influenza A Virus Infection *. *J. Biol. Chem.* **2012**, *287*, 35324–35332.

(38) Müller, K. H.; Kainov, D. E.; El Bakkouri, K.; Saelens, X.; De Brabander, J. K.; Kittel, C.; Samm, E.; Muller, C. P. The Proton Translocation Domain of Cellular Vacuolar ATPase Provides a Target for the Treatment of Influenza A Virus Infections. *Br. J. Pharmacol.* **2011**, *164*, 344–357.

(39) Chen, H.-W.; Cheng, J. X.; Liu, M.-T.; King, K.; Peng, J.-Y.; Zhang, X.-Q.; Wang, C.-H.; Shrestha, S.; Schooley, R. T.; Liu, Y.-T. Inhibitory and Combinatorial Effect of Diphyllin, a v-ATPase Blocker, on Influenza Viruses. *Antiviral Res.* **2013**, *99*, 371–382.

(40) Martinez-Lopez, A.; Persaud, M.; Chavez, M. P.; Zhang, H.; Rong, L.; Liu, S.; Wang, T. T.; Sarafianos, S. G.; Diaz-Griffero, F. Glycosylated Diphyllin as a Broad-Spectrum Antiviral Agent against Zika Virus. *EBioMedicine* **2019**, *47*, 269–283.

(41) Zhang, H.-J.; Rumschlag-Booms, E.; Guan, Y.-F.; Wang, D.-Y.; Liu, K.-L.; Li, W.-F.; Nguyen, V. H.; Cuong, N. M.; Soejarto, D. D.; Fong, H. H. S.; Rong, L. Potent Inhibitor of Drug-Resistant HIV-1 Strains Identified from the Medicinal Plant *Justicia Gendarussa*. *J. Nat. Prod.* **2017**, *80*, 1798–1807.

(42) Lindstrom, A. R.; Anantpadma, M.; Baker, L.; Raghavendra, N. M.; Davey, R.; Davisson, V. J. Phenotypic Prioritization of Diphyllin Derivatives That Block Filo-Viral Cell Entry by Vacuolar (H⁺)-ATPase Inhibition. *ChemMedChem* **2018**, *13*, 2664–2676.

(43) Stefanik, M.; Strakova, P.; Haviernik, J.; Miller, A. D.; Ruzek, D.; Eyer, L. Antiviral Activity of Vacuolar ATPase Blocker Diphyllin against SARS-CoV-2. *Microorganisms* **2021**, *9*, 471.

(44) König, R.; Stertz, S.; Zhou, Y.; Inoue, A.; Hoffmann, H.-H.; Bhattacharyya, S.; Alamares, J. G.; Tscherne, D. M.; Ortigoza, M. B.; Liang, Y.; Gao, Q.; Andrews, S. E.; Bandyopadhyay, S.; De Jesus, P.; Tu, B. P.; Pache, L.; Shih, C.; Orth, A.; Bonamy, G.; Miraglia, L.; Ideker, T.; García-Sastre, A.; Young, J. A. T.; Palese, P.; Shaw, M. L.; Chanda, S. K. Human Host Factors Required for Influenza Virus Replication. *Nature* **2010**, *463*, 813–817.

(45) Hu, C.-M. J.; Chen, Y.-T.; Fang, Z.-S.; Chang, W.-S.; Chen, H.-W. Antiviral Efficacy of Nanoparticulate Vacuolar ATPase Inhibitors against Influenza Virus Infection. *Int. J. Nanomed.* **2018**, *Volume 13*, 8579–8593.

(46) Hu, C.-M. J.; Chang, W.-S.; Fang, Z.-S.; Chen, Y.-T.; Wang, W.-L.; Tsai, H.-H.; Chueh, L.-L.; Takano, T.; Hohdatsu, T.; Chen, H.-W. Nanoparticulate Vacuolar ATPase Blocker Exhibits Potent Host-Targeted Antiviral Activity against Feline Coronavirus. *Sci. Rep.* **2017**, *7*, No. 13043.

(47) Dahlmann, F.; Biedenkopf, N.; Babler, A.; Jahnen-Dechent, W.; Karsten, C. B.; Gnirß, K.; Schneider, H.; Wrensch, F.; O'Callaghan, C. A.; Bertram, S.; Herrler, G.; Becker, S.; Pöhlmann, S.; Hofmann-Winkler, H. Analysis of Ebola Virus Entry Into Macrophages. *J. Infect. Dis.* **2015**, *212*, S247–S257.

(48) Wahl-Jensen, V.; Kurz, S.; Feldmann, F.; Buehler, L. K.; Kindrachuk, J.; DeFilippis, V.; da Silva Correia, J.; Früh, K.; Kuhn, J. H.; Burton, D. R.; Feldmann, H. Ebola Virus Attachment and Entry into

Human Macrophages Profoundly Effects Early Cellular Gene Expression. *PLoS Neglected Trop. Dis.* **2011**, *5*, No. e1359.

(49) Martinez, O.; Johnson, J. C.; Honko, A.; Yen, B.; Shabman, R. S.; Hensley, L. E.; Olinger, G. G.; Basler, C. F. Ebola Virus Exploits a Monocyte Differentiation Program To Promote Its Entry. *J. Virol.* **2013**, *87*, 3801–3814.

(50) Saeed, M. F.; Kolokoltsov, A. A.; Freiberg, A. N.; Holbrook, M. R.; Davey, R. A. Phosphoinositide-3 Kinase-Akt Pathway Controls Cellular Entry of Ebola Virus. *PLoS Pathog.* **2008**, *4*, No. e1000141.

(51) Breiden, B.; Sandhoff, K. Emerging Mechanisms of Drug-Induced Phospholipidosis. *Biol. Chem.* **2019**, *401*, 31–46.

(52) Klumperman, J.; Raposo, G. The Complex Ultrastructure of the Endolysosomal System. *Cold Spring Harbor Perspect. Biol.* **2014**, *6*, No. a016857.

(53) Nelson, E. A.; Dyall, J.; Hoenen, T.; Barnes, A. B.; Zhou, H.; Liang, J. Y.; Michelotti, J.; Dewey, W. H.; DeWald, L. E.; Bennett, R. S.; Morris, P. J.; Guha, R.; Klumpp-Thomas, C.; McKnight, C.; Chen, Y.-C.; Xu, X.; Wang, A.; Hughes, E.; Martin, S.; Thomas, C.; Jahrling, P. B.; Hensley, L. E.; Olinger, G. G.; White, J. M. The Phosphatidylinositol-3-Phosphate 5-Kinase Inhibitor Apilimod Blocks Filoviral Entry and Infection. *PLoS Neglected Trop. Dis.* **2017**, *11*, No. e0005540.

(54) Choy, C. H.; Saffi, G.; Gray, M. A.; Wallace, C.; Dayam, R. M.; Ou, Z.-Y. A.; Lenk, G.; Puertollano, R.; Watkins, S. C.; Botelho, R. J. Lysosome Enlargement during Inhibition of the Lipid Kinase PIKfyve Proceeds through Lysosome Coalescence. *J. Cell Sci.* **2018**, *131*, No. jcs213587.

(55) Sbrissa, D.; Naisan, G.; Ikononov, O. C.; Shisheva, A. Apilimod, a Candidate Anticancer Therapeutic, Arrests Not Only PtdIns(3,5)P2 but Also PtdIns5P Synthesis by PIKfyve and Induces Bafilomycin A1-Reversible Aberrant Endomembrane Dilation. *PLoS One* **2018**, *13*, No. e0204532.

(56) D'Arrigo, A.; Bucci, C.; Toh, B. H.; Stenmark, H. Microtubules Are Involved in Bafilomycin A1-Induced Tubulation and Rab5-Dependent Vacuolation of Early Endosomes. *Eur. J. Cell Biol.* **1997**, *72*, 95–103.

(57) Li, S.; Liang, Z.; Li, J.; Zhang, X.; Zheng, R.; Zhao, C. Update on Naturally Occurring Novel Arylnaphthalenes from Plants. *Phytochem. Rev.* **2020**, *19*, 337–403.

(58) Shi, D.-K.; Zhang, W.; Ding, N.; Li, M.; Li, Y.-X. Design, Synthesis and Biological Evaluation of Novel Glycosylated Diphyllin Derivatives as Topoisomerase II Inhibitors. *Eur. J. Med. Chem.* **2012**, *47*, 424–431.

(59) Wang, A. C.; Pham, H. T.; Lipps, J. M.; Brittain, S. M.; Harrington, E.; Wang, Y.; King, F. J.; Russ, C.; Pan, X.; Hoepfner, D.; Tallarico, J.; Feng, Y.; Jain, R. K.; Schirle, M.; Thomas, J. R. Previously Uncharacterized Vacuolar-Type ATPase Binding Site Discovered from Structurally Similar Compounds with Distinct Mechanisms of Action. *ACS Chem. Biol.* **2019**, *14*, 20–26.

(60) Rowland, A. A.; Chitwood, P. J.; Phillips, M. J.; Voeltz, G. K. ER Contact Sites Define the Position and Timing of Endosome Fission. *Cell* **2014**, *159*, 1027–1041.

(61) Bohdanowicz, M.; Balkin, D. M.; De Camilli, P.; Grinstein, S. Recruitment of OCRL and Inpp5B to Phagosomes by Rab5 and APPL1 Depletes Phosphoinositides and Attenuates Akt Signaling. *Mol. Biol. Cell* **2012**, *23*, 176–187.

(62) Aldrich, L. N.; Kuo, S.-Y.; Castoreno, A. B.; Goel, G.; Kuballa, P.; Rees, M. G.; Seashore-Ludlow, B. A.; Cheah, J. H.; Latorre, I. J.; Schreiber, S. L.; Shamji, A. F.; Xavier, R. J. Discovery of a Small-Molecule Probe for V-ATPase Function. *J. Am. Chem. Soc.* **2015**, *137*, 5563–5568.

(63) Zoncu, R.; Bar-Peled, L.; Efeyan, A.; Wang, S.; Sancak, Y.; Sabatini, D. M. MTORC1 Senses Lysosomal Amino Acids Through an Inside-Out Mechanism That Requires the Vacuolar H⁺-ATPase. *Science* **2011**, *334*, 678–683.

(64) Anantpadma, M.; Kouznetsova, J.; Wang, H.; Huang, R.; Kolokoltsov, A.; Guha, R.; Lindstrom, A. R.; Shtanko, O.; Simeonov, A.; Maloney, D. J.; Maury, W.; LaCount, D. J.; Jadhav, A.; Davey, R. A. Large Scale Screening and Identification of Novel Ebolavirus and

Marburgvirus Entry Inhibitors. *Antimicrob. Agents Chemother.* **2016**, *60*, 4471–4481.

(65) Suzuki, Y.; Kotoura, M.; Yashima, S.; Wu, H.; Nakano, T.; Sano, K. Measuring Dengue Virus RNA in the Culture Supernatant of Infected Cells by Real-Time Quantitative Polymerase Chain Reaction. *J. Vis. Exp.* **2018**, *141*, No. e58407.